MULTIPLE INPUT MULTIPLE OUTPUT TRANSMISSION TECHNIQUES AND LINK ADAPTATION IN WIRELESS SYSTEMS WITH DUAL-POLARIZED ANTENNAS

by

Yakup Kılıç

B.S, Electronics and Communication Engineering, Yıldız Technical University, 2007

Submitted to the Institute for Graduate Studies in
Science and Engineering in partial fulfillment of
the requirements for the degree of
Master of Science

Graduate Program in FBE Program for which the Thesis is Submitted
Boğaziçi University
2009

MULTIPLE INPUT MULTIPLE OUTPUT TRANSMISSION TECHNIQUES AND LINK ADAPTATION IN WIRELESS SYSTEMS WITH DUAL-POLARIZED ANTENNAS

APPROVED BY:

Assist. Prof. Mutlu Koca (Thesis Supervisor)	.....
Prof. Emin Anarım (Thesis Co-supervisor)	.....
Assoc. Prof. Mehmet Akar	.....
Assoc. Prof. Fatih Alagöz	.....
Assist. Prof. Kerem Harmancı	.....

DATE OF APPROVAL: .....

ACKNOWLEDGEMENTS

First of all, I would like to thank to my supervisors Assist. Prof. Mutlu Koca and Prof. Emin Anarım for their invaluable help and encouragement. This thesis can not be accomplished without their guidance. Apart from the thesis, I also appreciate the suggestions of Assist. Prof. Mutlu Koca in order to find a Phd position.

I am also thankful to Assoc. Prof. Mehmet Akar, Assoc. Prof. Fatih Alagöz and Assist. Prof. Kerem Harmancı for being part of my thesis jury. Furthermore, I would like to thank Dr. Tolga Kurt for his contributions to the thesis.

The long and painful hours spent on this thesis became an entertainment with Sinan Tekincan, Alparslan Çil, Temuçin Som, Erdem Aytaç, Fatih Arslan, Kemal Davaslıoğlu, Salim Bahçeci, Nazlı Güney and Serkan Mülayim. Also, I would like to give special thanks to Berfu Güley Gören for her support during the graduate study.

Last but not least, I would like to thank to my parents for their eternal support during my education life.

This thesis is supported by TUBITAK 2210 Graduate Student Scholarship program and TUBITAK KARIYER project with number 105E077.

ABSTRACT

MULTIPLE INPUT MULTIPLE OUTPUT TRANSMISSION TECHNIQUES AND LINK ADAPTATION IN WIRELESS SYSTEMS WITH DUAL-POLARIZED ANTENNAS

The use of dual-polarized antennas theoretically double the number of virtual antennas used in the system. On the other hand, the correlation effects and the cross-polar discrimination (XPD) deteriorates the system performance. When considering 2×2 dual-polarized multiple input multiple output (MIMO) communication system, a virtual 4×4 system is obtained where the hybrid MIMO options can also be carried out to maximize detection performance and multiplexing gain of the system. In this thesis, we propose a new hybrid approach and present performance analysis of a dual-polarized 2×2 system for space-time-block coding (STBC), spatial multiplexing (SM) and hybrid schemes. We also present simulation results for these multi-antenna signalling techniques under various XPD and correlation scenarios. Both the theoretical analysis and the simulation results show a significant performance gain by joint utilization of space, time and polarization diversity over the uni-polarized MIMO systems. However, the complexity of the system increases rapidly with respect to modulation order in the case of optimal detection at the receiver. In this regard, we propose a low complexity iterative receiver based on joint use of linear minimum mean squared error (MMSE) equalization and soft interference cancellation (SIC) process. In order to have efficient link adaptation, we design an unique receiver that has capability to detect symbols belonging to these four MIMO options. When combining four MIMO options with modulation and coding schemes (MCS) introduced in 802.11n and WiMAX, a transmission channel can be fully utilized with an proper adaptive switching mechanism. Therefore, as an example we employ the standard link adaptation technique for IEEE 802.11n standard. Simulation results indicate that a double throughput and significant range improvement can be achieved via the use of dual-polarized antenna elements.

ÖZET

ÇİFT YÖNLÜ KUTUPLANMIŞ ANTENLİ KABLOSUZ SİSTEMLERDE ÇOK GİRDİLİ ÇOK ÇIKTILI GÖNDERİM TEKNİKLERİ VE LİNK UYARLAMA

Çift-yönlü kutuplanmış anten kullanımı kuramsal olarak sistemdeki sanal anten sayısını iki katına çıkarır. Ancak ilinti etkileri ve çapraz kutupsama ayrımsama (ÇKA) sistemin başarımını düşürücü yönde etki yapar. 2×2 çok girdili çok çıktılı (ÇGÇÇ) iletişim sistemi ele alındığında, sistemin algılama başarımını ve çoğullama kazancını en yüksek yapmak için karma ÇGÇÇ seçeneklerinin de kullanılabileceği bir sanal 4×4 sistem elde edilir. Bu tezde yeni bir karma yaklaşım önerilmiş, çift-yönlü kutuplanmış 2×2 ÇGÇÇ sistemde uzay-zaman-blok kodları (UZBK), uzamsal çoğullama ve karma şemaların kullanımıyla elde edilen başarım analizi sunulmuştur. Aynı zamanda, bu dört çoklu anten işaretleşme tekniği için farklı ÇKA ve ilinti senaryolarına göre benzetim sonuçları sunulmuştur. Hem kuramsal analiz hem de benzetim sonuçlarına göre uzay-zaman ve kutuplama çeşitlemesinin birlikte kullanımıyla tek-yönlü kutuplanmış anten sistemlerine kıyasla ciddi bir başarım artışı elde edilir. Fakat, en uygun algılama tekniği kullanıldığında, sistemin karmaşıklığı kipleme derecesine bağlı olarak artar. Bu nedenle, doğrusal en düşük ortalama karesel hata (EDOKH) denkleştirme ve yumuşak bilgi giderme işlemi tabanlı düşük karmaşıklı bir alıcı önerilmiştir. Link uyarlamanın verimliliğini arttırmak açısından, bu dört farklı ÇGÇÇ gönderim tekniğine ait sembolleri algılama yeteneğine sahip tek bir alıcı tasarlanmıştır. Dört ÇGÇÇ seçeneği, IEEE 802.11n ve WiMAX sistemlerindeki kipleme ve kodlama yapılarıyla birleştirildiğinde, uygun bir uyarlanır anahtarlama mekanizmasıyla iletim kanalı tam olarak doldurulabilir. Bu nedenle, örnek olarak temel link uyarlama tekniği IEEE 802.11n standardı için uygulanmıştır. Benzetim sonuçlarına göre çift-yönlü kutuplanmış anten kullanımıyla, 802.11n sistemi için fiziksel katmanda birim zamanda gönderilen veri miktarı iki katına çıkarılmış ve kapsama alanında ciddi bir artış elde edilmiştir.

TABLE OF CONTENTS

LIST OF FIGURES

LIST OF TABLES

LIST OF SYMBOLS/ABBREVIATIONS

$\otimes$	Kronecker product
$\mathbf{1}$	All-one matrix
$(a)^*$	Complex conjugate of a
$\mathbf{A}^H$	Conjugate transpose of $\mathbf{A}$
$\mathbf{A}^T$	Transpose of $\mathbf{A}$
$\mathbf{A}^\dagger$	Moore-Penrose pseudo inverse of $\mathbf{A}$
$\mathbf{C}_{\tilde{\mathbf{y}}}$	Channel correlation matrix
$\text{diag}(a_1, a_2, ..., a_n)$	$n \times n$ diagonal matrix with (m, m)th element $= a_m$
d^2_{min}	Minimum distance between symbols for the given constellation
d_s	The delay spread
$\mathbf{e}$	Erroneously detected signal
$\text{E}\{a\}$	Expected value of a
exp()	Exponential function
f_s	Input symbol rate
$h_{i,j}$	Channel coefficient between the ith transmit and the jth receive antennas
$\overline{h}_{i,j}$	Elements of fixed components of the channel matrix
$\widetilde{h}_{i,j}$	Elements of variable components of the channel matrix
$\mathbf{H}$	Channel matrix
$\overline{\mathbf{H}}$	Fixed component of the channel matrix
$\widetilde{\mathbf{H}}$	Variable component of the channel matrix
$\mathbf{I}$	Identity matrix
I_0	Modified Bessel function of the first kind
K	K-factor
L_{GI}	Length guard interval
L_p	The number of channel taps
log()	Logarithmic function
M	Modulation order

$\mathbf{n}$	Noise vector for additive white Gaussian noise
$n(\epsilon_i)$	Relative frequency of an error event
$\overline{N}_e$	The average number of nearest neighbors
N_{ite}	The number of iterations
N_t	Number of transmit antennas
N_r	Number of receiver antennas
$p(.)$	Probability density function
P_A	Probability of error for dual-polarized 2×1 Alamouti
P_S	Probability of error for dual-polarized 2×1 SM
r	Receive correlation coefficient
$\mathbf{r}$	Received signal vector
$r(\mathbf{A})$	Rank of matrix $\mathbf{A}$
$\mathbf{R}_{\text{tx}}$	Correlation matrix at the transmitter side
$\mathbf{R}_{\text{rx}}$	Correlation matrix at the receiver side
s	Spatial correlation coefficient
S	Symbol alphabet
$s(\epsilon_i)$	Scalar symbol error events
t	Transmit correlation coefficient
T_s	Symbol duration
$\mathbf{x}$	The transmitted signal matrix
XPD	Value of XPD-factor
vec(.)	For a matrix $\mathbf{A} = [\mathbf{a}_1\ \mathbf{a}_2\ .\ .\ \mathbf{a}_n]$ where $\mathbf{a}_i$ is a column vector of $\mathbf{A}$, vec(.) operator returns a vector $\mathbf{b} = [\mathbf{a}_1^T\ \mathbf{a}_2^T\ .\ .\ \mathbf{a}_n^T]$
w_c	The coherence bandwidth
w_i	MMSE filter coefficients
Z	Number of subcarriers
α	Channel parameter related to the XPD defined for the variable component of the channel
$\alpha_{i,j,l}$	Correlated channel coefficients for the lth tap
α_f	Channel parameter related to the XPD defined for the fixed component of the channel
δ	Subcarrier spacing

$\delta(t)$	Dirac delta function
λ_a	A priori information
λ_e	Extrinsic information
λ_p	A posteriori probability
$\Pi(.)$	Interleaving matrix
ρ_{ij}^{rx}	Complex receive correlation coefficient
ρ_{ij}^{tx}	Complex transmit correlation coefficient
σ^2	Noise variance
τ_l	The time delay of the lth path

AARF	Adaptive automatic rate fallback
ACK	Acknowledgement
ARF	Automatic rate fallback
AWGN	Additive white Gaussian noise
BCJR	Bahl, Cocke, Jelinek, Raviv
BER	Bit error rate
BPSK	Binary phase shift keying
CARA	Collision aware rate adaptation
CDMA	Code division multiple access
CP	Cyclic prefix
CSI	Channel state information
DFT	Discrete Fourier transform
EDGE	Enhanced data-rates for GSM evolution
FDE	Frequency domain equalization
ICI	Inter-carrier interference
IDFT	Inverse discrete Fourier transform
i.i.d	Independent identically distributed
IPTV	Internet protocol television
ISI	Inter-symbol interference
LAN	Local area network
LOG-MAP	Logarithmic maximum a-posteriori probability

LOS	Line of sight
MAC	Medium access control
MAI	Multiple access interference
MAP	Maximum a-posteriori probability
MAX-LOG-MAP	Maximum logarithmic maximum a-posteriori probability
MCS	Modulation and coding scheme
MIMO	Multiple input multiple output
ML	Maximum likelihood
MMSE	Minimum mean squared error
QAM	Quadratic amplitude modulation
QPSK	Quadratic phase shift keying
OFDM	Orthogonal frequency division multiplexing
PDF	Probability density function
PHY	Physical
PSK	Phase shift keying
ROM	Read only memory
SIC	Soft interference cancellation
SISO	Single input single output (Chapters 2-3)
SISO	Soft input soft output (Chapter 4)
SM	Spatial multiplexing
SNR	Signal-to-noise ratio
STBC	Space-time-block coding
VOIP	Voice over internet protocol
XPD	Cross polar discrimination
WIMAX	Worldwide interoperability for microwave access
WLAN	Wireless local area networks
ZF	Zero-forcing

1. INTRODUCTION

Demands for the higher transmission rates in a reliable way is increased as wireless networks start to offer video and voice transmission in addition to the data transmission. Thus, recently, next-generation wireless networks have emerged to offer higher transmission rates with less transmission errors through the use of multiple antennas. Multiple antenna systems increase the reliability and spectral efficiency of the system through the use of diversity techniques and SM scheme, respectively. Diversity techniques are widely used to reduce the effect of multi-path fading. The probability of all the replicas of the same information symbol experiencing the same fading decreases as the number of diversity branches increase. In [1], a basic transmit diversity scheme is developed for two transmit antennas, while in [2] the diversity gain is increased with using more than two antennas and employing orthogonal codes. In these works, the channel is assumed to be uncorrelated and at the receiver maximum-likelihood detection is employed together with combining techniques. On the other hand, the spectral efficiency of the system is increased by employing spatial multiplexing (SM) [3] which permits the opening of multiple spatial data pipes between transmitter and receiver without any additional bandwidth or power requirement.

MIMO systems introduce a spatial dimension to existing rate adaptation algorithms that implies to decide MIMO transmission type, STBC, spatial multiplexing or hybrid approaches, as well as modulation and coding type. However, in MIMO systems, correlations may occur between channel coefficients due to insufficient antenna spacing and the scattering properties of the transmission environment. This may lead to significant degradation in system performance. In this regard, adding more antennas to the base-station and/or the subscriber unit require more spatial dimension at the base-station and/or the subscriber unit in order to have an uncorrelated channel between antenna elements. Hence, it would not be feasible to design higher order MIMO systems in small handsets. On the other hand the use of dual-polarized antenna elements is introduced as a space and cost-effective alternative, that is used to transmit information symbols through vertical and horizontal polarizations without any additional

power and bandwidth requirement. In communication with dual-polarized antenna elements, the information streams are sent through vertical and horizontal polarizations of the antenna elements at the same time and frequency.

However as pointed out in [4], imperfections of transmit and/or receive antennas and XPD factor, which is the power ratio of the co-polar and cross-polar components, degrades the system performance considerably. In [5], a system employing one dual-polarized antenna at the transmitter and one dual-polarized antenna at the receiver is presented and the error performance of 2-antenna SM and STBC transmission schemes are derived for this virtual MIMO system. Notice that, in [5], a single-input single-output (SISO) system is enabled with MIMO capabilities through the use of dual-polarized antennas. In this thesis, we present the performance of MIMO systems employing dual-polarized antennas under different correlation parameters and XPD factors over correlated Rayleigh fading channels. In this regard, not only the transmit and receive antenna correlations and the XPD factor, but also a spatial correlation is included in the system analysis.

In IEEE 802.11n and WiMAX systems, 2×1 and 2×2 antenna configurations are used with Alamouti and SM transmission techniques, however, although it is defined in the standards, higher order MIMO systems are not used due to the space problem. The system throughput is controlled by both these two MIMO options and modulation and coding schemes (MCS) defined in the standards. However, when dual-polarized antenna elements are used at both link ends, a virtual 4×4 MIMO system is obtained where the hybrid MIMO options can also be carried out to maximize detection performance and multiplexing gain of the system. In this respect, we propose a new hybrid method, namely 1×SM + 1×Alamouti, and adopt another hybrid transmission technique (2×Alamouti) to dual-polarized MIMO communication systems. Totally, we could employ four transmission strategies to this virtual MIMO system. These are; 2×2 dual-polarized STBC, 2×2 dual-polarized SM, 2×Alamouti and 1×SM + 1×Alamouti. Notice that this range of transmission alternatives over the same physical system allow an efficient trade-off between the diversity gain and the multiplexing gain that the overall system can achieve. Even though the results can be generalized to any

number of transmit/receive antennas, throughout the thesis only a 2×2 dual-polarized antenna system is considered where it is shown to have better performance than the 2×2 uni-polarized antenna systems.

In combination of virtual 4×4 MIMO system with MCS's including large constellation sizes, a tremendous computational effort is required when the optimal detection techniques are employed at the receiver, especially for SM and hybrid transmission techniques. On the other hand, we need a low complexity but an effective receiver. Therefore, in this thesis we propose a low complexity receiver structure based on joint use of linear MMSE detection and SIC process. Notice that, in order to have efficient link adaptation, we develop an universal receiver that has capability to change detection parameters according to the dual-polarized MIMO transmission mode in order to detect symbols, adequately.

Recently, a lot of research efforts have done in order to suppress undesired transmission effects through low complexity iterative equalization methods based on the joint use of linear MMSE filtering and SIC process. For instance, in [6]-[8] multiple access interference are cancelled out for CDMA systems while in [9]-[10] ISI effects are suppressed for single antenna systems. However, when the channel memory length is large, employing equalization at time domain would require a considerable computational effort due to the matrix inversion. Therefore, frequency domain equalization is introduced in the literature and through [11]-[14] low complexity iterative frequency domain equalization is studied. Moreover, equalization task is performed at frequency domain in OFDM systems where frequency-selective fading channels become frequency-flat fading channels by sending the symbols through orthogonal subcarriers [15],[16]. By adding at least channel length cyclic prefix to the system, OFDM technology solves the ISI problem. Due to that reason, OFDM is used as a standard technique in IEEE 802.11n WiMAX systems.

When combining four dual-polarized MIMO transmission techniques with MCS's introduced in IEEE 802.11n and WiMAX standards, a transmission channel can be fully utilized via a proper adaptive switching mechanism. In this regard, we em-

ploy the standard link adaptation technique, given in [17], where SNR information is defined as a link quality indicator and the transmission parameters are adopted to the current channel conditions according to the SNR knowledge. We also show the performance improvement over conventional systems. As an example we consider IEEE 802.11n standard throughout our simulations. Simulation results indicate that a double throughput and significant range improvement is obtained through the use of dual-polarized antenna elements.

1.1. Thesis Outline

In Chapter 2, we introduce the MIMO transmission concept, including transmission techniques and the channel models. This chapter may also be regarded as literature review part. In Chapter 3, a channel model is developed for 2×2 dual-polarized MIMO system based on the model developed in [5]. Error performance analysis of four dual-polarized MIMO transmission techniques are derived analytically. And simulation results are given for various dual-polarized channel parameters. In Chapter 4, an effective low complexity iterative receiver is developed for 2×2 dual-polarized MIMO system. The performance of this receiver is shown for different transmission techniques introduced in Chapter 3. In Chapter 5, a standard link adaptation algorithm is employed to 2×2 dual-polarized MIMO system. The simulation results are given for IEEE 802.11n links according to the average SNR information provided by the receiver. A look-up table is built and throughput and range increase is shown at the end of this chapter. Finally, the concluding remarks are drawn out in Chapter 6.

2. MIMO COMMUNICATION SYSTEMS

The use of multiple antennas both at the transmitter and the receiver, which is commonly referred as MIMO, is a popular research area in wireless communications literature because of its reliability and spectral efficiency. With the growth of applications that demand better quality of services, higher throughput and bandwidth, MIMO communication has emerged as a promising technology. The ideas behind the MIMO communication are either creating a multiple data pipes to increase the data rate and/or adding diversity to improve the reliability. The former idea is achieved through use of SM technique [3], which offers multiplexing gain, with effective detection algorithms at the receiver. However the latter idea is achieved with STBC schemes introduced in [1, 18].

2.1. Analytical MIMO Channel Models

It is important to know the characteristic behaviour of the MIMO channel in order to design good detection algorithms at the receiver. For a $N_t \times N_r$ MIMO systems where N_t and N_r denote the number of transmit and receive antennas, respectively, the MIMO channel matrix at a given time instant given as below,

$$\mathbf{H} = \begin{bmatrix} h_{1,1} & h_{2,1} & h_{3,1} & \dots & h_{N_t,1} \\ h_{1,2} & h_{2,2} & h_{3,2} & \dots & h_{N_t,2} \\ \vdots & \vdots & & \ddots & \vdots \\ h_{1,N_r} & h_{2,N_r} & h_{3,N_r} & \dots & h_{N_t,N_r} \end{bmatrix} \tag{2.1}$$

where $h_{i,j}$ is the channel coefficient between the ith transmit and jth receive antenna. In most of the works, those coefficients are chosen independent identically distributed (i.i.d) complex Gaussian random variables, however antenna spacings and scattering properties of the environment introduce correlation. Whereas rich scattering in the environment and adequate antenna spacings ensures the decorrelation of the MIMO channel elements.

2.1.1. Rayleigh Fading Channels

When the spatial distance between antennas and angular spreading is large enough, the channel coefficients are assumed to be uncorrelated. Also, if all the channel elements have the same average power, then the correlation matrix is proportional to unity. In this case, the complex fading coefficients $h_{i,j}$'s are assumed to be a zero-mean unit variance complex Gaussian random variable with independent real and imaginary parts. Equivalently, $h_{i,j}$'s have uniform phase and Rayleigh amplitude.

However, as it is pointed out in [19], limited angular spread and limited distance between antennas cause the channels become correlated. Furthermore, if there is a strong LOS component, the channel statistics become Rician distributed. In addition, the use of polarization diversity creates gain imbalances between elements of the MIMO channel matrix since the vertical and horizontal polarizations have different propagation characteristics.

Based on the measurement results, a simple stochastic MIMO channel model is developed in [20], referred as Kronecker product model in the literature, that takes into account the correlation effects both at the transmitter and the receiver side. However they assume that all antenna elements have the same polarization and radiation pattern which is not the case in polarization diversity. They separate the correlation effects at both link ends and show in a matrix form as $\mathbf{R}_{\text{tx}}$ and $\mathbf{R}_{\text{rx}}$ for the transmitter and the receiver sides, respectively. And the general spatial correlation for the MIMO radio channel is shown as Kronecker product of the $\mathbf{R}_{\text{tx}}$ and $\mathbf{R}_{\text{rx}}$ and is given by

$$\mathbf{R}_{\text{MIMO}} = \mathbf{R}_{\text{tx}} \otimes \mathbf{R}_{\text{rx}}. \tag{2.2}$$

The elements of the $N_t \times N_t$ transmit and the $N_r \times N_r$ receive correlation matrices are given as

$$\begin{aligned} \rho_{ij}^{\text{tx}} &= < h_{m,i}, h_{m,j} >, \\ \rho_{ij}^{\text{rx}} &= < h_{i,m}, h_{j,m} > \end{aligned} \tag{2.3}$$

where ρ_{ij}^{tx} and ρ_{ij}^{rx} denote the complex transmit and receive correlation coefficients, respectively. $< x, y >$ is the power correlation coefficient between the complex random variables x and y given as [20],

$$< x, y >= \frac{\mathrm{E}\{|x|^2|y|^2\} - \mathrm{E}\{|x|^2\}\mathrm{E}\{|y|^2\}}{\sqrt{\mathrm{E}\{|x|^4 - (\mathrm{E}\{|x|^2\})^2\}\mathrm{E}\{|y|^4 - (\mathrm{E}\{|y|^2\})^2\}}} \tag{2.4}$$

2.1.2. Rician Fading Channels

When there is not any obstruct between the transmitter and the receiver, typically a LOS case, received signal consists of a direct wave and number of waves. In this case, channel coefficients would have non-zero mean because of the strong direct path. The sum of direct signal together with a Rayleigh distributed scattered signal results in a signal with a Rician envelope distribution. Under the assumption that the total average signal power is normalized to unity, the pdf of the Rician distribution is given as [21],

$$p(a) = 2a(1+K)e^{-K-(1+K)a^2 I_0(2a\sqrt{K(K+1)})} \quad a \geq 0 \tag{2.5}$$

where I_0 is the modified Bessel function of the first kind and zero order and K is the Rician factor which denotes the power ratio of the direct and scattered signal components. For $K = 0$ Rician distribution becomes the Rayleigh distribution. For higher values of K, the channel approaches to the LOS channel. When K goes to infinity, the channel is more like AWGN channel [21].

Thus, MIMO channel matrix can be decomposed into a LOS and NLOS component as [22],

$$\mathbf{H} = \sqrt{\frac{K}{K+1}}\overline{\mathbf{H}} + \sqrt{\frac{1}{K+1}}\widetilde{\mathbf{H}} \tag{2.6}$$

where $\overline{\mathbf{H}}$ stands for the fixed component of the channel (LOS component) and $\widetilde{\mathbf{H}}$ stands for the variable component of the channel (NLOS component).

2.1.3. Dual-Polarized Channels

As mentioned in section 2.1.1, low levels of physical separation between antennas introduce correlation that results a degradation in system performance. Physical separation must be up to λ and 30λ [23] between the transmitter and the receiver antenna elements, respectively, in order to achieve significant multiplexing and diversity gain. On the other hand, with the recent amendments in the wireless technology, there is much attention to small hand held devices. Thus, polarization diversity scheme is first proposed in [23], as a promising alternative to space diversity systems. The technique has recently become of interest, due to the fact that it does not require any increase in bandwidth and any physical separation between the antenna elements.

In polarization diversity scheme, signals are transmitted through horizontal and vertical polarizations at the same time and frequency without any requirement of spatial separation. Typically, two polarization schemes are used: horizontal/vertical ($0°/90°$) or slanted ($+45°/-45°$) as shown in Figure 2.1.

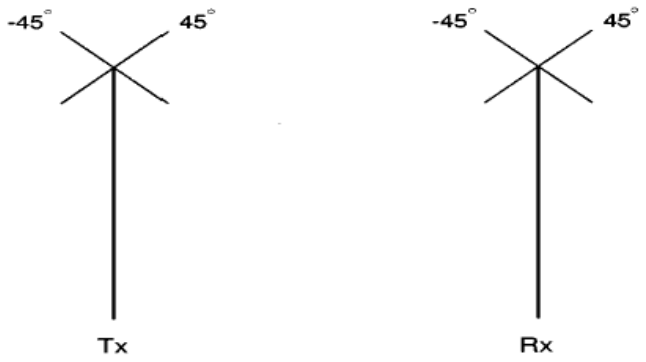

Figure 2.1. Schematic of dual-polarized slanted antenna setup both at the transmitter (T_x) and the receiver (R_x) side [5].

Ideally, there should be no transmission from a vertically polarized antenna to a horizontally polarized antenna. However two factors, known as cross-polar isolation and cross-polar ratio, introduce decorrelation in the system and results a cross-polar transmission. Cross-polar isolation is the result of imperfect isolation between the

orthogonal feeds. And the cross-polar ratio occurs when the environment is rich in scattering. The combination of these two factors results in the term XPD. Thus as stated in [4], XPD is result of cross-polar isolation in the LOS environments since there is not any scattered component. On the other hand, in NLOS scenarios, assuming there is a perfect cross-polar isolation between antennas then only the scattering effects in the environment change the polarization state of the transmitted signal.

A more detailed dual-polarized channel model is given in section 3.1 for 2×2 dual-polarized systems.

2.1.4. Frequency-Selective Fading Channels

In narrow band wireless communication systems, we deal with frequency non-selective flat fading channels since the coherence bandwidth is larger than the bandwidth of the signal. The term, coherence bandwidth, represents the frequency interval over which two frequencies of a signal are likely to experience correlated fading. The coherence bandwidth is defined as

$$w_c = \frac{2\pi}{d_s}(rd/s) \tag{2.7}$$

where d_s denotes the delay spread of the channel which is the duration between the arrival time of the first multi-path component (i.e LOS component) and the last multi-path component. Due to the fact that, the symbol period becomes smaller relative to the channel delay spread or in other words, coherence bandwidth becomes smaller than the signal bandwidth, then frequency-selective fading occurs in wide band communication systems.

The time-variant impulse response at time t to an impulse applied at time $t - \tau$ for a multipath fading channel with L_p different taps is given as [21]

$$h(t;\tau) = \sum_{l=1}^{L_p} h^{t,l}\delta(t - \tau_l) \tag{2.8}$$

where $h^{t,l}$ and τ_l are the complex amplitude and time delay of the lth path, respectively. In general, the sampled impulse response $h(t;\tau)$ has an infinite length but in most analysis, it is truncated to an effective length which contains number of taps with most of the power [24].

Since the symbol duration is smaller than the channel delay spread, ISI occurs. In the case of ISI, as the complexity of the ML decoding is prohibitively high, adaptive equalization techniques are proposed as a lower complexity alternative for single antenna systems in order to mitigate the effects of ISI [21]. However in MIMO systems, this technique also brings high computational complexity to the receiver. Therefore, as an alternative approach, OFDM is widely used technique in order to suppress the ISI which is discussed in section 2.3.

2.2. MIMO Transmission Techniques

Mainly, MIMO offers two types of gain which are called diversity and multiplexing gains. Diversity gain mitigates the fading and improves the performance of the system by sending independent copies of the transmitted signal through different antennas. By increasing the number of independent copies of the transmitted signal, the probability of at least one of the signal not experiencing deep fade decreases. Thus, the reliability of the transmission and throughput increase. On the other hand, multiplexing gain offers higher transmission rates under rich scattering environment, in which the decorrelation of MIMO channels is guaranteed, by sending different symbols through different antennas at the same time.

2.2.1. Space-Time Coding

Alamouti scheme [1] is basic space-time code structure to achieve full transmit diversity with two transmit antennas and number of receive antennas. Regardless of modulation size; in the first symbol period, two modulated symbols are transmitted while in the second period, complex conjugate of these two symbols are transmitted as shown in Figure 2.2. While the transmission rate does not change, the diversity order is

doubled. In general, the transmission matrix for space-time block code is $N_t \times p$ matrix

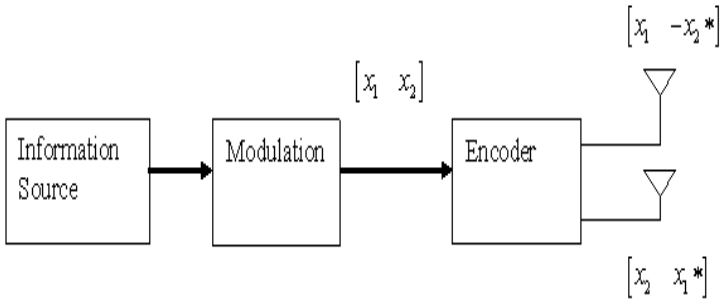

Figure 2.2. Block representation of the Alamouti space-time encoder.

where N_t is the number of transmitter antenna elements and p denotes the number of time periods for transmission of one block of symbols. The transmitted signal matrix for Alamouti scheme is

$$\mathbf{x} = \begin{bmatrix} x_1 & -x_2^* \\ x_2 & x_1^* \end{bmatrix}. \tag{2.9}$$

For 2×2 system, channel matrix is defined as,

$$\mathbf{H} = \begin{bmatrix} h_{1,1} & h_{2,1} \\ h_{1,2} & h_{2,2} \end{bmatrix} \tag{2.10}$$

where channel coefficients are i.i.d complex Gaussian random variables. Equivalently, the received signal samples for each receiver in the first and second signalling interval can be written as,

$$\begin{aligned} r_1(2t) &= h_{1,1}x_1(2t) + h_{2,1}x_2(2t) + n_1(2t) \\ r_1(2t+1) &= -h_{1,1}x_2^*(2t+1) + h_{2,1}x_1^*(2t) + n_1(2t+1) \\ r_2(2t) &= h_{1,2}x_1(2t) + h_{2,2}x_2(2t) + n_2(2t) \\ r_2(2t+1) &= -h_{1,2}x_2^*(2t+1) + h_{2,2}x_1^*(2t) + n_2(2t+1) \end{aligned}$$

where $r_k(t)$ and $n_k(t)$ are the received signal samples and additive noise at the kth receiver antenna elements at the tth time interval. Notice that, we simply obtain the conjugate of the symbols in the second signalling interval by taking the conjugate of the noise terms. In matrix form, it can be written as [25]

$$\underbrace{\begin{bmatrix} r_1(2t) \\ r_1^*(2t+1) \\ r_2(2t) \\ r_2^*(2t+1) \end{bmatrix}}_{\mathbf{r}_p} = \underbrace{\begin{bmatrix} h_{1,1} & h_{2,1} \\ h_{2,1}^* & -h_{1,1}^* \\ h_{1,2} & h_{2,2} \\ h_{2,2}^* & -h_{1,2}^* \end{bmatrix}}_{\mathbf{H}_p} \begin{bmatrix} x_1 \\ x_2 \end{bmatrix} + \underbrace{\begin{bmatrix} n_1(2t) \\ n_1^*(2t+1) \\ n_2(2t) \\ n_2^*(2t+1) \end{bmatrix}}_{\mathbf{n}_p}. \tag{2.11}$$

As Alamouti proposes in his original paper, we multiply $\mathbf{r}_p$ by $\mathbf{H}_p^H$ in the receiver to get,

$$\begin{aligned} \widehat{x}_1 &= (|h_{1,1}^2| + |h_{2,1}^2| + |h_{1,2}^2| + |h_{2,2}^2|)x_1 + v_1 \\ \widehat{x}_2 &= (|h_{1,1}^2| + |h_{2,1}^2| + |h_{1,2}^2| + |h_{2,2}^2|)x_2 + v_2. \end{aligned} \tag{2.12}$$

where $\widehat{x}_1$ and $\widehat{x}_2$ are the combiner output for the symbols x_1 and x_2, respectively, and $\mathbf{v}_p = \begin{bmatrix} v_1 & v_2 \end{bmatrix}^T$ in which the elements are obtained from $\mathbf{v}_p = \mathbf{H}_p^H \mathbf{n}_p$. And then using maximum-likelihood detection at the receiver, we estimate the transmitted symbols x_1 and x_2 as in [1]. This alternative representation enables us to design a unique system that runs the different transmission schemes in a framework.

The Alamouti scheme achieves the full diversity with a very simple receiver structure. The orthogonality between the sequences generated by the two transmit antenna elements is the key feature of the scheme. This scheme can be generalized to arbitrary number of transmit antennas with keeping this orthogonality principle. In [2] and [26], various rates space-time-block codes are designed for complex and real constellations.

Throughout the thesis, we use the G_4 code proposed in [2], which is given below,

$$\mathbf{x} = \begin{bmatrix} x_1 & x_2 & x_3 & x_4 \\ -x_2 & x_1 & -x_4 & x_3 \\ -x_3 & x_4 & x_1 & -x_2 \\ -x_4 & -x_3 & x_2 & x_1 \\ x_1^* & x_2^* & x_3^* & x_4^* \\ -x_2^* & x_1^* & -x_4^* & x_3^* \\ -x_3^* & x_4^* & x_1^* & -x_2^* \\ -x_4^* & -x_3^* & x_2^* & x_1^* \end{bmatrix}^T . \tag{2.13}$$

Notice that in eight signalling interval, four symbols are transmitted through transmitter antenna elements resulting the rate-1/2 code.

2.2.2. Spatial Multiplexing

Spatial multiplexing scheme achieves multiplexing gain by sending independent information symbols across the parallel spatial channels at the same time. As shown in the Figure 2.3, the physical data rate of the system increases proportional to number of independent data streams transmitted on each transmitter antenna without additional power or bandwidth consumption. Unlike the Alamouti scheme, the multiple

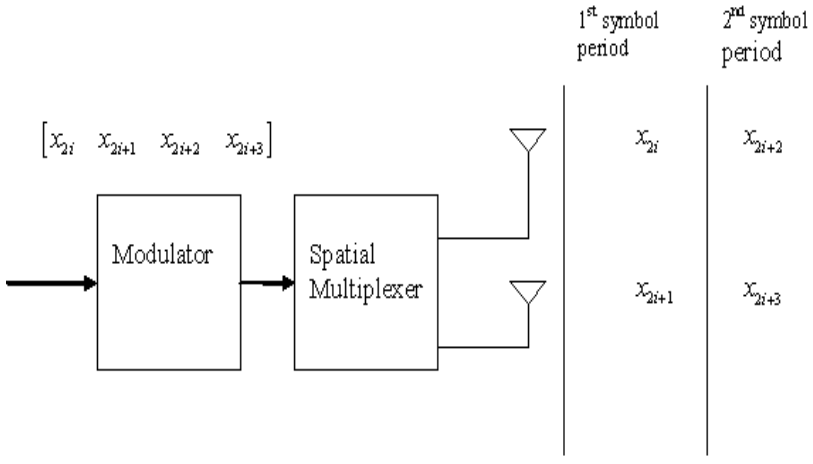

Figure 2.3. Block Representation of the spatial multiplexing scheme.

transmitted data streams interfere with each other at the receiver. Hence, in order to reliably detect the transmitted signal, we need the condition that $N_t \leq N_r$.

Let us consider 2×2 MIMO system employing spatial multiplexing scheme through transmitter antennas. Considering uncorrelated fading channel, the channel matrix can be defined as (2.10). The received signal can be expressed as below

$$\mathbf{r} = \mathbf{H}\mathbf{x} + \mathbf{n} \tag{2.14}$$

where $\mathbf{x} = \begin{bmatrix} x_1 & x_2 \end{bmatrix}^T$ is the transmitted signal vector and $\mathbf{n} = \begin{bmatrix} n_1 & n_2 \end{bmatrix}^T$ is the zero-mean i.i.d Gaussian noise vector with variance of $N_0/2$ for each element. At each time instant, receiver uses ML decoding in order to detect the transmitted signal properly according to (2.15).

$$\widetilde{\mathbf{x}} = \arg\min_{\widetilde{x}_i \in S} \|\mathbf{r} - \mathbf{H}\widetilde{\mathbf{x}}\|^2 \tag{2.15}$$

Although ML decoding is an optimum detection technique for spatial multiplexing, the complexity of the scheme grows exponentially with respect to the number of the transmit antennas and modulation order. Let M denotes the modulation order, the complexity of the ML decoding is M^{N_t}. In order to reduce this complexity, sub-optimum linear receivers based on zero-forcing (ZF) and MMSE filtering are proposed in the literature.

2.2.2.1. Zero-Forcing Linear Receiver. In the ZF receiver architecture, the received signal is multiplied by the inverse of the channel matrix, in order to suppress the interference caused by other transmitted symbols as shown in (2.16)

$$\widetilde{\mathbf{x}}_{\mathrm{ZF}} = \mathbf{H}^{\dagger}\mathbf{r} \tag{2.16}$$

where $\mathbf{H}^{\dagger} = (\mathbf{H}^H\mathbf{H})^{-1}\mathbf{H}^H$ is Moore-Penrose pseudo inverse of the channel matrix $\mathbf{H}$. Notice that ZF filtering converts the channel into N_t SISO channels, therefore each

symbol can be detected using ML decoding separately. Thus, the complexity of the ZF decoding is similar to the single antenna ML decoding. On the other hand, there is performance degradation due to the noise enhancement.

2.2.2.2. MMSE Linear Receiver. Recall that employing ZF algorithm at the receiver suppresses the interference and creates parallel SISO channels but also enhances the noise. A possible solution to this noise enhancement problem could be using classical MMSE filtering technique where the filtering coefficients are obtained according to

$$\mathbf{z}_f = (\mathbf{H}^H\mathbf{H} + \frac{1}{\sigma^2}\mathbf{I}_{N_t})^{-1}\mathbf{H} \tag{2.17}$$

where σ^2 is noise variance and $\mathbf{I}_{N_t}$ is $N_t \times N_t$ identity matrix. Notice that, $\mathbf{H}^H\mathbf{H} \ll \frac{1}{\sigma^2}\mathbf{I}_{N_t}$ at low SNR region, therefore MMSE filtering outperforms ZF filtering in this region and reduces to the matched filtering, however in high SNR region MMSE filter approaches to the ZF filtering.

In Figure 2.4, simulation results are given for ZF, MMSE and ML receivers for spatial multiplexing scheme using QPSK modulation under the uncorrelated Rayleigh fading channel. Notice that there is a huge performance gap between ML receiver and ZF or MMSE receivers. Performance gain is about 16 dB at 10^{-4} bit-error-rate threshold. Furthermore, performance of both detection techniques approaches to the SISO performance at high SNR region which means both scheme can perfectly cancel out the interference and create multiple SISO channels.

2.3. OFDM Basics

In OFDM communication system, high-rate data stream is splitted into lower rate data streams that are transmitted over a number of subcarriers simultaneously. Thus, the symbol duration increases for the lower rate parallel subcarriers and becomes smaller than the channel delay spread. Equivalently, coherence bandwidth becomes larger than the bandwidth of the symbol. Therefore, by using OFDM, frequency-

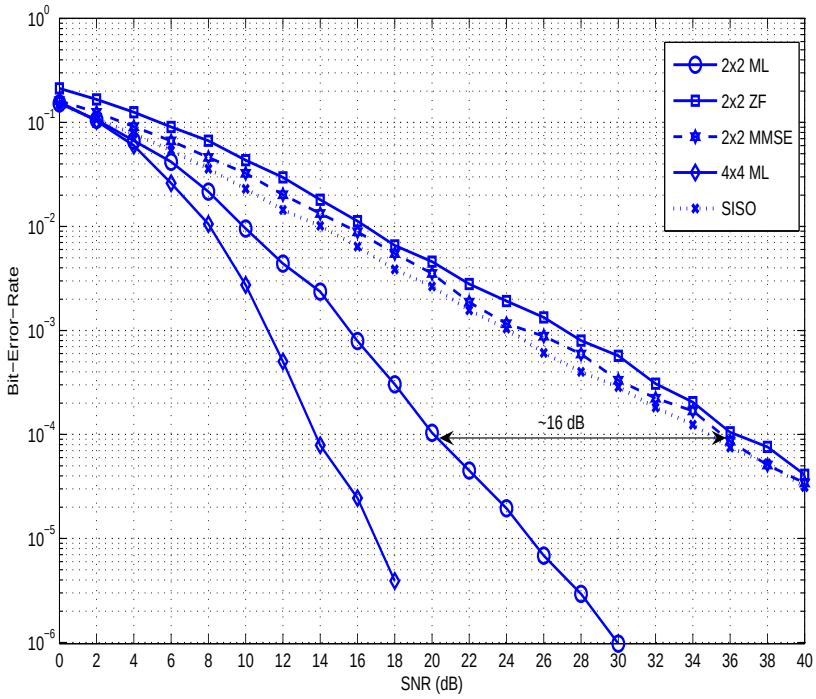

Figure 2.4. Performance of ZF, MMSE and ML receivers for spatial multiplexing scheme in i.i.d Rayleigh fading channels.

selective channel becomes parallel frequency-flat subchannels.

Let us assume that data symbols have a duration that $T_s = \frac{1}{f_s}$ where f_s is the input symbol rate. Each OFDM frame consists of Z coded symbols. After the serial-to-parallel conversion, Z parallel data are modulated by Z subcarrier frequency denoted by $f_0, f_1, ..., f_{Z-1}$. In order to make the frequencies orthogonal, the subcarrier spacing is set to $\delta = \frac{1}{ZT_s}$. Since the carriers are orthogonal, data can be detected using each of these closely spaced carriers without any interference from the other carriers. OFDM modulated signal is the inverse discrete Fourier transform (IDFT) of the original data stream, which recovered at the receiver using simply DFT [21], [24], [27]. With efficient discrete Fourier transform algorithms, the implementation complexity of the OFDM system is very low.

In order to fully eliminate the ISI, a guard interval is appended between consecutive OFDM frames. The guard interval is chosen larger than the expected channel

delay spread such that multipath of the one symbol can not interfere with the next symbol. The guard interval is chosen as the copy of the last L_{GI} samples of the OFDM frame. As it is shown in [27], the guard interval may consist of no signal at all, but in that case subcarriers become no more orthogonal and thus inter carrier interference (ICI) is appeared.

3. DUAL-POLARIZED MIMO SYSTEMS

As we already discussed in Chapter 2, MIMO transmission techniques, such as STBC or SM, are known to achieve significant diversity or multiplexing gains, respectively. Most of the analysis have an assumption that the channel between the transmitter and the receiver is uncorrelated. However, in the literature the performance degradation due to the correlation effect is realized, and new methods are still under investigation. For instance, in [28], new robust space-time codes are introduced for correlated MIMO channels to increase diversity order and it is shown that the performance of the new codes under correlated channels approaches to the performance of the orthogonal codes under i.i.d channels for SM scheme. Moreover, the correlation effect is studied through [20] and [29] and channel models, which are supported by measurement results, are developed.

Notice that, one of the main reason for correlation in MIMO systems is the poor antenna antenna spacings between antenna elements. On the other hand, the use of dual-polarized antennas instead of uni-polarized antennas is a cost and space-effective alternative, where two spatially separated uni-polarized antennas are replaced by a single dual-polarized antenna. Communication with dual-polarized antennas require the transmission of two independent symbols on the same bandwidth and the same carrier frequency at the same time by using two orthogonal polarizations. In [5], a general channel model is developed for dual-polarized SISO system and the error performance SM and STBC transmission schemes are derived for the 2×2 virtual MIMO system. In [30], combined spatial multiplexing and Alamouti scheme is used as an hybrid approach between orthogonal polarizations of the each dual-polarized antenna to increase multiplexing gain of the system while keeping the performance of conventional Alamouti scheme. To the best of our knowledge, this work is first to consider dual-polarized MIMO systems before our work.

In this chapter, we present the performance of MIMO systems employing dual-polarized antennas under different correlation parameters and XPD factors over corre-

lated Rayleigh fading channels for the the following four transmission schemes:

- 2×2 dual-polarized STBC,
- 2×2 dual-polarized SM,
- $2\times$ Alamouti (employing two Alamouti schemes from both antennas),
- $1\times$Alamouti + $1\times$SM (employing Alamouti at one antenna and SM at the other).

The error performances of these schemes are presented with theoretical analysis and simulation results. Notice that this range of transmission alternatives over the same physical system provide an efficient trade-off between the diversity gain and the multiplexing gain that the overall system can achieve. Even though the results can be generalized to any number of transmit/receive antennas, however throughout this chapter only a 2×2 and 2×1 dual-polarized antenna systems are considered where it is shown to have better performance than the 2×2 and 2×1 uni-polarized antenna systems, respectively. The use of dual-polarized antennas leads the way to achieving diversity and multiplexing gains at a high rate, when combined with the link adaptation algorithms which are envisioned for next generation wireless communication systems with MIMO capabilities (i.e IEEE 802.11n, Wimax).

3.1. Channel Model

In this work the channel model, adopted in [5], is developed for two dual-polarized antennas at the transmitter and the receiver as shown in Fig. 3.1. The received signal is defined as,

$$\mathbf{r} = \mathbf{H}\mathbf{x} + \mathbf{n} \tag{3.1}$$

where $\mathbf{x}$ is the transmitted signal vector, is chosen from a complex constellation such that the average energy of the constellation element is one, and $\mathbf{n}$ is a vector of zero mean i.i.d Gaussian components with variance $N_0/2$ for each element. The channel

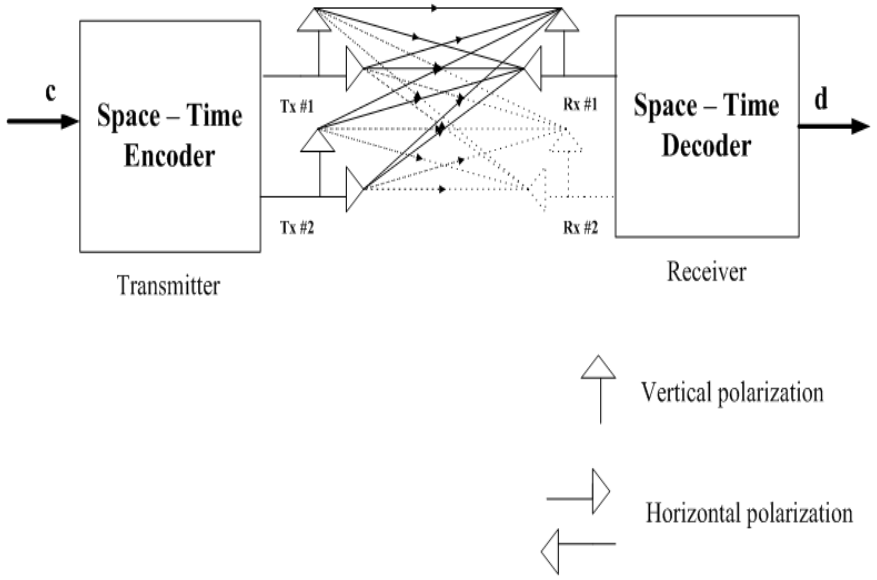

Figure 3.1. Block diagram of dual-polarized antenna system

matrix for a 2×2 dual-polarized system is defined as,

$$\mathbf{H} = \begin{bmatrix} h_{1v,1v} & h_{1h,1v} & h_{2v,1v} & h_{2h,1v} \\ h_{1v,1h} & h_{1h,1h} & h_{2v,1h} & h_{2h,1h} \\ h_{1v,2v} & h_{1h,2v} & h_{2v,2v} & h_{2h,2v} \\ h_{1v,2h} & h_{1h,2h} & h_{2v,2h} & h_{2h,2h} \end{bmatrix} \tag{3.2}$$

where subscript kv and kh denote vertical and horizontal polarization of the kth antenna element, respectively. The channel matrix can be decomposed into the sum of an average and a variable component as,

$$\mathbf{H} = \sqrt{\frac{K}{K+1}}\overline{\mathbf{H}} + \sqrt{\frac{1}{K+1}}\widetilde{\mathbf{H}} \tag{3.3}$$

where the elements of $\overline{\mathbf{H}}$, denoted as $\overline{h}_{i,j}$, represents the fixed components of the channel matrix and the elements of $\widetilde{\mathbf{H}}$, denoted as $\widetilde{h}_{i,j}$, are zero-mean circularly symmetric complex Gaussian random variables whose variances depend on the propagation environment and the characteristics of the antennas at both link ends.

The relationships between the fixed and the variable channel components are

given in (3.4) and (3.5) with an assumption in (3.6) for a 2×1 dual-polarized system.

$$\begin{aligned} \mathrm{E}\{|\overline{h}_{1v,1v}|^2\} &= \mathrm{E}\{|\overline{h}_{1h,1h}|^2\} = \mathrm{E}\{|\overline{h}_{2v,1v}|^2\} = \mathrm{E}\{|\overline{h}_{2h,1h}|^2\} = 1, \\ \mathrm{E}\{|\overline{h}_{1v,1h}|^2\} &= \mathrm{E}\{|\overline{h}_{1h,1v}|^2\} = \mathrm{E}\{|\overline{h}_{2v,1h}|^2\} = \mathrm{E}\{|\overline{h}_{2h,1v}|^2\} = \alpha_f, \end{aligned} \tag{3.4}$$

$$\begin{aligned} \mathrm{E}\{|\widetilde{h}_{1v,1v}|^2\} &= \mathrm{E}\{|\widetilde{h}_{1h,1h}|^2\} = \mathrm{E}\{|\widetilde{h}_{2v,1v}|^2\} = \mathrm{E}\{|\widetilde{h}_{2h,1h}|^2\} = 1, \\ \mathrm{E}\{|\widetilde{h}_{1v,1h}|^2\} &= \mathrm{E}\{|\widetilde{h}_{1h,1v}|^2\} = \mathrm{E}\{|\widetilde{h}_{2v,1h}|^2\} = \mathrm{E}\{|\widetilde{h}_{2h,1v}|^2\} = \alpha, \end{aligned} \tag{3.5}$$

$$\mathrm{E}\{\widetilde{h}_{1h,1h}\widetilde{h}^*_{1v,1v}\} = \mathrm{E}\{\widetilde{h}_{1v,1h}\widetilde{h}^*_{1h,1v}\} = \mathrm{E}\{\widetilde{h}_{2h,1h}\widetilde{h}^*_{2v,1v}\} = \mathrm{E}\{\widetilde{h}_{2v,1h}\widetilde{h}^*_{2h,1v}\} = 0. \tag{3.6}$$

Since it would be hard to follow long expressions, we simply write the equations for a 2×1 system and then get the channel correlation matrix for a 2×2 system. In the equations, $\mathrm{E}\{.\}$ denotes the expectation operator and $0 \leq \alpha_f \leq 1$ is defined for the fixed component of the channel. Also α is defined as $\alpha = \frac{1}{\mathrm{XPD}}$ in $[0, 1]$, where XPD is the power ratio of the co-polar and cross-polar components. thus greater values of α yield good cross-polar discrimination. The Rician K-factor, which denotes the ratio between the power of the LOS and the power of the NLOS components, is defined as

$$\begin{aligned} \mathbf{K} &= \begin{bmatrix} K_{1v,1v} & K_{1h,1v} & K_{2v,1v} & K_{2h,1v} \\ K_{1v,1h} & K_{1h,1h} & K_{2v,1h} & K_{2h,1h} \end{bmatrix}^T, \\ K_{1v,1v} &= K_{2v,1v} = K_{1h,1h} = K_{2h,1h} = \frac{\alpha_f}{\alpha}, \\ K_{1h,1v} &= K_{2h,1v} = K_{1v,1h} = K_{2v,1h} = K \end{aligned} \tag{3.7}$$

where $K = 0$ represents the pure Rayleigh condition and superscript $\{.\}^T$ stands for transpose operation. Normalized receive and transmit correlation coefficients are de-

fined in (3.8).

$$\begin{aligned} t &= \frac{\mathrm{E}\{\widetilde{h}_{1h,1h}\widetilde{h}^*_{1v,1h}\}}{\sqrt{\alpha}} = \frac{\mathrm{E}\{\widetilde{h}_{1h,1v}\widetilde{h}^*_{1v,1v}\}}{\sqrt{\alpha}} = \frac{\mathrm{E}\{\widetilde{h}_{2h,1h}\widetilde{h}^*_{2v,1h}\}}{\sqrt{\alpha}} = \frac{\mathrm{E}\{\widetilde{h}_{2h,1v}\widetilde{h}^*_{2v,1v}\}}{\sqrt{\alpha}} \\ r &= \frac{\mathrm{E}\{\widetilde{h}_{1h,1h}\widetilde{h}^*_{1h,1v}\}}{\sqrt{\alpha}} = \frac{\mathrm{E}\{\widetilde{h}_{1v,1h}\widetilde{h}^*_{1v,1v}\}}{\sqrt{\alpha}} = \frac{\mathrm{E}\{\widetilde{h}_{2h,1h}\widetilde{h}^*_{2h,1v}\}}{\sqrt{\alpha}} = \frac{\mathrm{E}\{\widetilde{h}_{2v,1h}\widetilde{h}^*_{2v,1v}\}}{\sqrt{\alpha}} \end{aligned} \quad (3.8)$$

Since we are dealing with more than one dual-polarized antenna, we also consider spatial correlation between antennas. Therefore parameter s, which denotes the spatial correlation between antennas, is defined as

$$s = \mathrm{E}\{\widetilde{h}_{k,l}\widetilde{h}^*_{m,l}\} \quad (3.9)$$

where $l = 1v, 1h$; $k = 1v, 1h$ and $m = 2v, 2h$. In order to determine the effects of transmit, receive and spatial correlations and XPD factor, $\mathbf{y} = \mathrm{vec}(\mathbf{H})$ is defined and decomposed into a fixed and a variable component as

$$\overline{\mathbf{y}} = \mathrm{vec}\left(\sqrt{\frac{K}{1+K}}\overline{\mathbf{H}}\right), \quad (3.10)$$

$$\widetilde{\mathbf{y}} = \mathrm{vec}\left(\sqrt{\frac{1}{1+K}}\widetilde{\mathbf{H}}\right). \quad (3.11)$$

Since the channel matrix $\mathbf{H}$ is Gaussian, the vector $\mathbf{y}$ is also Gaussian and all the channel realizations can be characterized by the eigenvalues of the 8×8 correlation matrix, which is nonnegative-definite and defined by

$$\mathbf{C}_{\widetilde{\mathbf{y}}} = \mathrm{E}\{\widetilde{\mathbf{y}}\widetilde{\mathbf{y}}^H\} = \mathbf{\Pi}\mathbf{\Sigma}\mathbf{\Pi}^H \quad (3.12)$$

where $\mathbf{\Sigma} = \mathrm{diag}\{\lambda_i\}_{i=1}^8$. In the equations, $\{.\}^H$ stands for the conjugate transpose operation. And for any length-l vector input, diag$\{.\}$ operation returns a $l \times l$ square matrix whose diagonal elements are the elements of the input vector. The correlation

matrix for a 2×1 dual-polarized system is given in (3.13).

$$\mathbf{C}_{\widetilde{\mathbf{y}}_{\mathbf{4\times 2}}} = \begin{bmatrix} 1 & t^*\sqrt{\alpha} & s & s & r^*\sqrt{\alpha} & 0 & s & s \\ t\sqrt{\alpha} & \alpha & s & s & 0 & r^*\sqrt{\alpha} & s & s \\ s & s & 1 & t^*\sqrt{\alpha} & s & s & r^*\sqrt{\alpha} & 0 \\ s & s & t\sqrt{\alpha} & \alpha & s & s & 0 & r^*\sqrt{\alpha} \\ r\sqrt{\alpha} & 0 & s & s & \alpha & t^*\sqrt{\alpha} & s & s \\ 0 & r\sqrt{\alpha} & s & s & t\sqrt{\alpha} & 1 & s & s \\ s & s & r\sqrt{\alpha} & 0 & s & s & \alpha & t^*\sqrt{\alpha} \\ s & s & 0 & r\sqrt{\alpha} & s & s & t\sqrt{\alpha} & 1 \end{bmatrix} \tag{3.13}$$

And finally the correlation matrix for a 2×2 dual-polarized system is defined as

$$\mathbf{C}_{\widetilde{\mathbf{y}}_{\mathbf{4\times 4}}} = \begin{bmatrix} \mathbf{C}_{\widetilde{\mathbf{y}}_{\mathbf{4\times 2}}} & s\mathbf{1}_{\mathbf{8\times 8}} \\ s\mathbf{1}_{\mathbf{8\times 8}} & \mathbf{C}_{\widetilde{\mathbf{y}}_{\mathbf{4\times 2}}} \end{bmatrix} \tag{3.14}$$

where $\mathbf{1}_{\mathbf{8\times 8}}$ refers to a 8×8 all-one matrix. Note that the above matrix is defined in terms of transmit (t), receive (r) and spatial (s) correlations and α which is related to the XPD. By changing these parameters, we can obtain different channel conditions for NLOS case by

$$\widetilde{\mathbf{y}}^H = \mathbf{\Pi}^{\frac{1}{2}} \mathbf{\Sigma}^{\frac{1}{2}} \mathrm{vec}(\mathbf{H}_w) \tag{3.15}$$

where $\mathbf{H}_w$ is an i.i.d channel matrix.

3.2. Error Performance of Space-Time-Block Coding

For the virtual 4-antenna system, we employ the rate-1/2 complex G_4 code given in [2] as

$$\mathbf{x} = \begin{bmatrix} x_1 & x_2 & x_3 & x_4 \\ -x_2 & x_1 & -x_4 & x_3 \\ -x_3 & x_4 & x_1 & -x_2 \\ -x_4 & -x_3 & x_2 & x_1 \\ x_1^* & x_2^* & x_3^* & x_4^* \\ -x_2^* & x_1^* & -x_4^* & x_3^* \\ -x_3^* & x_4^* & x_1^* & -x_2^* \\ -x_4^* & -x_3^* & x_2^* & x_1^* \end{bmatrix}^T . \tag{3.16}$$

These symbols are mapped to the horizontal and vertical polarizations of the dual-polarized antennas. Maximum-ratio combining is employed at the receiver in order to obtain the decision metric,

$$\widetilde{\mathbf{x}}_{\mathbf{k}} = \sum_{j=0}^{N_r-1} \sum_{i=0}^{3} |h_{i,j}|^2 \mathbf{x}_{\mathbf{k}} + \boldsymbol{\eta} \tag{3.17}$$

where $\boldsymbol{\eta}$ is a zero-mean Gaussian random variable and N_r is the number of receive antennas. In [18] assuming ideal channel state information (CSI), the probability of transmitting $\mathbf{x}$ and deciding erroneously in favor of $\mathbf{e}$ is approximated by

$$\begin{aligned} &P(\mathbf{x} \rightarrow \mathbf{e} \mid h_{i,j}, i = 1, 2, ..., N_t, j = 1, 2, ..., N_r) \\ &\qquad \leq \exp\left(-\mathbf{y}\mathbf{D}(\mathbf{x}, \mathbf{e})\mathbf{y}^{\mathbf{H}}\chi\right) \end{aligned} \tag{3.18}$$

where $\chi = \frac{E_s}{4N_0}$, and

$$\mathbf{D}(\mathbf{x},\mathbf{e}) = \begin{bmatrix} \mathbf{A}(\mathbf{x},\mathbf{e}) & \mathbf{0} & \dots & \mathbf{0} \\ \mathbf{0} & \mathbf{A}(\mathbf{x},\mathbf{e}) & \dots & \mathbf{0} \\ \vdots & \vdots & \ddots & \vdots \\ \mathbf{0} & \mathbf{0} & \dots & \mathbf{A}(\mathbf{x},\mathbf{e}) \end{bmatrix} \tag{3.19}$$

is a $N_t N_r \times N_t N_r$ matrix where $\mathbf{0}$ denotes the $N_t \times N_t$ all-zero matrix. $\mathbf{A}(\mathbf{x},\mathbf{e})$ can be defined as $\mathbf{A}(\mathbf{x},\mathbf{e}) = \mathbf{B}(\mathbf{x},\mathbf{e})\mathbf{B}(\mathbf{x},\mathbf{e})^H$ where $\mathbf{B}(\mathbf{x},\mathbf{e})$ shows the distance between each symbol on the constellation defined for l symbol as

$$\mathbf{B}(\mathbf{x},\mathbf{e}) = \begin{bmatrix} x_1^1 - e_1^1 & x_2^1 - e_2^1 & \dots & x_l^1 - e_l^1 \\ x_1^2 - e_1^2 & x_2^2 - e_2^2 & \dots & x_l^2 - e_l^2 \\ \vdots & \vdots & \ddots & \vdots \\ x_1^n - e_1^n & x_2^n - e_2^n & \dots & x_l^n - e_l^n \end{bmatrix}. \tag{3.20}$$

From (3.18) the probability that the receiver decodes the transmitted symbol in error for a given channel realization is approximated and upper bounded by

$$P(\mathbf{x} \to \mathbf{e}|\mathbf{H}) \leq \overline{N}_e \exp\left(-\chi d_{min}^2 \|\mathbf{y}\|^2\right) \tag{3.21}$$

where $\overline{N}_e$ and d_{min}^2 are the average number of nearest neighbors and minimum distance of the constellation. For the pure Rayleigh case where K=0, (3.21) can be written as

$$P(\mathbf{x} \to \mathbf{e}|\mathbf{H}) \leq \overline{N}_e \prod_{i=0}^{r(\mathbf{C}_{\tilde{\mathbf{y}}})-1} \frac{1}{1 + \chi d_{min}^2 \lambda_i} \tag{3.22}$$

where $r(\mathbf{C}_{\tilde{\mathbf{y}}})$ denotes the rank of the correlation matrix.

The correlation matrix is orthogonal if and only if $s = r = t = 0$ and $\alpha = 1$. In this case the channel becomes the i.i.d Rayleigh fading MIMO channel. Thus, the error probability is minimized for spatially uncorrelated fading and in the absence of polarization diversity. Thus a 4×4 uni-polarized system has higher performance than

a 2×2 dual-polarized system. In order to get an accurate computation, the expression in (3.22) is scaled by an empirically determined constant as in [5].

3.3. Error Performance of Spatial Multiplexing

In SM scheme, because we are interested in using two dual-polarized antennas both at the transmitter and the receiver, the symbol stream is divided into four sub-streams and then transmitted simultaneously from the two orthogonal polarizations. Assuming perfect channel knowledge, maximum-likelihood detection is employed at the receiver according to the following equation

$$\widetilde{\mathbf{x}} = \arg \min_{\widetilde{x}_i \in S} \|\mathbf{r} - \mathbf{H}\widetilde{\mathbf{x}}\|^2. \tag{3.23}$$

Let ϵ indicates the error between $\mathbf{x}$ and $\tilde{\mathbf{x}}$, for a given channel realization $\mathbf{H}$ using the Chernoff bound, the error probability is given below

$$P(\epsilon|\mathbf{H}) \leq \exp\left(-\chi\|\mathbf{x}_e\|^2\right) \tag{3.24}$$

where $\chi = \frac{E_s}{N_0}$ and $\mathbf{x}_e = \mathbf{H}\epsilon$ which can be decomposed into fixed and variable component as

$$\overline{\mathbf{x}}_{\mathbf{e}} = \sqrt{\frac{K}{K+1}}\overline{\mathbf{H}}\epsilon, \tag{3.25}$$

$$\widetilde{\mathbf{x}}_{\mathbf{e}} = \sqrt{\frac{1}{K+1}}\widetilde{\mathbf{H}}\epsilon. \tag{3.26}$$

Upon defining $\mathbf{C}_{\widetilde{\mathbf{e}}} = \mathrm{E}\{\widetilde{\mathbf{x}}_{\mathbf{e}}\widetilde{\mathbf{x}}_{\mathbf{e}}^H\} = \mathbf{\Pi}\mathbf{\Sigma}\mathbf{\Pi}^H$ where the diagonal elements of $\mathbf{\Sigma}$ are defined as λ_i. And the pairwise error probability averaged over all the channel realizations for Rayleigh fading channel can be expressed as

$$P(\epsilon) \leq \prod_{i=0}^{r(\mathbf{C}_{\tilde{\mathbf{z}}})-1} \frac{1}{1+\chi\lambda_i}. \tag{3.27}$$

The average symbol error rate of SM is then estimated as

$$P(\epsilon) \leq \sum_{\epsilon_i} n(\epsilon_i) P(\epsilon_i) s(\epsilon_i) \tag{3.28}$$

where considering BPSK transmission, $n(\epsilon_i)$ denotes the relative frequency of an error event and is given as

$$n(\epsilon_i) = \frac{w(\epsilon_i, 1v) w(\epsilon_i, 1h) w(\epsilon_i, 2v) w(\epsilon_i, 2h)}{240} \tag{3.29}$$

with

$$w(\epsilon_i, j) = \begin{cases} 2 & \text{If } \epsilon_i = 0 \text{ (error-free case)} \\ 1 & \text{If } \epsilon_i = \pm 2 \end{cases}$$

and $s(\epsilon_i)$ represents the number of scalar symbol errors with associated error event, as follow

$$s(\epsilon_i) = \begin{cases} 4 & \text{If error in all orthogonal polarizations,} \\ 3 & \text{If error in 3 orthogonal polarizations ,} \\ 2 & \text{If error in 2 orthogonal polarizations,} \\ 1 & \text{If error in any orthogonal polarization.} \end{cases}$$

3.4. Error Performance of Hybrid Transmission Techniques

In order to obtain diversity and multiplexing gains together, hybrid approaches combining transmit diversity and SM through the orthogonal polarizations can be employed in dual-polarized systems.

In this thesis, we propose an hybrid algorithm that employs Alamouti and SM schemes through the vertical and horizontal components, respectively, as shown in Fig. 3.2. Since each dual-polarized antenna elements is responsible for transmission

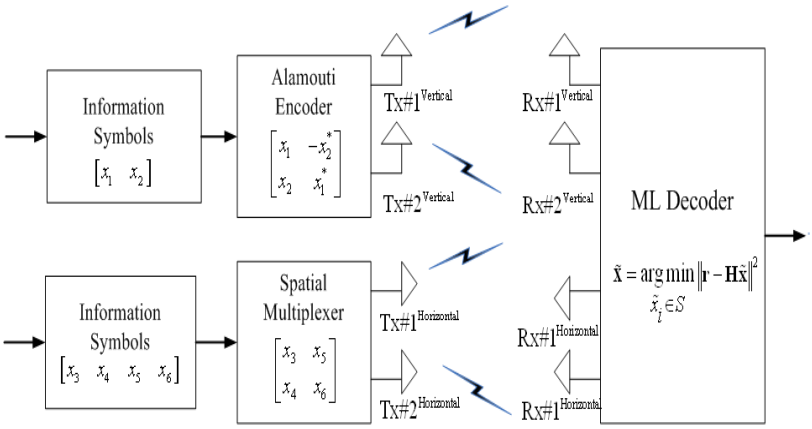

Figure 3.2. Block diagram of proposed hybrid dual-polarized antenna system

of Alamouti and SM coded symbols separately, throughout the thesis, we refer this hybrid structure as $1 \times$ SM & $1 \times$ Alamouti.

The transmitted signal matrix is shown below

$$\mathbf{x} = \begin{bmatrix} x_1 & -x_2^* \\ x_2 & x_1^* \\ x_3 & x_4 \\ x_5 & x_6 \end{bmatrix}. \tag{3.30}$$

Since vertical polarizations of the transmitter antennas used for the Alamouti coded signal and horizontal polarizations of the transmitter used for the spatially multiplexed signal our channel matrix slightly differ from (3.2). The channel matrix is defined as

$$\mathbf{H} = \begin{bmatrix} h_{1v,1v} & h_{2v,1v} & h_{1h,1v} & h_{2h,1v} \\ h_{1v,2v} & h_{2v,2v} & h_{1h,2v} & h_{2h,2v} \\ h_{1v,1h} & h_{2v,1h} & h_{1h,1h} & h_{2h,1h} \\ h_{1v,2h} & h_{2v,2h} & h_{1h,2h} & h_{2h,2h} \end{bmatrix}. \tag{3.31}$$

Employing the new $\mathbf{H}$ and $\mathbf{x}$, the received signal can be found according to (3.1). At the receiver, assuming perfect channel knowledge, maximum-likelihood detection is

employed according to the following decision metric,

$$\widetilde{\mathbf{x}} = \arg\min_{\widetilde{x}_i \in S} \|\mathbf{r} - \mathbf{H}\widetilde{\mathbf{x}}\|^2 \tag{3.32}$$

where $\widetilde{\mathbf{x}}$ is the detected symbol matrix in similar form to (3.30). $\widetilde{x}_i$'s ($i = 1, .., 6$) are chosen from a constellation set S which has complex symbols of an M-ary phase-shift keying or quadratic-amplitude modulation symbol alphabet. Notice that, in two signalling periods, six symbols are transmitted through the orthogonal polarizations of antenna elements. Thus, the physical data rate of the system increases by a factor of three.

The error performance of the system can be investigated separately for the vertically polarized and the horizontally polarized components where the Alamouti and the SM schemes are employed, respectively. Taking into consideration that there is a cross-polar transmission (i.e from vertically polarized antenna elements to horizontally polarized antenna elements) between orthogonal polarizations, the diversity order of the system increases due to the use of 2 dual-polarized antennas at the receiver. In this regard, we need to consider error performance of 1×2 dual-polarized Alamouti (P_{A}) and 1×2 dual-polarized SM (P_{S}) schemes. The error performance of P_{A} and P_{S} can be easily obtained from the equations (3.22) and (3.27), respectively. However notice that, since we originally have two dual-polarized antenna elements at the transmitter, transmitted signal power has to be divided by two while calculating P_{A} and P_{S}. Finally, the average symbol error rate for $1 \times$ SM & $1 \times$ Alamouti is obtained as below

$$P(\epsilon) \leq \frac{2P_{\mathrm{S}}}{3} + \frac{1P_{\mathrm{A}}}{3}. \tag{3.33}$$

A 2×Alamouti technique is also proposed in [30] for a 2×1 dual-polarized system where the aim is to double the throughput while having the performance of the Alamouti scheme. Here, two blocks of Alamouti coded signals are sent through vertical and horizontal components separately. In [30], as it is also proposed in [31], the ZF interference suppression technique is employed at the receiver. However in order to pro-

vide compatibility with other schemes, in our simulations we implement this scheme with maximum-likelihood detection without zero-forcing interference cancellation at the front end. The error performance of this scheme is given below,

$$P(\epsilon) \leq P_{\mathrm{A}}. \tag{3.34}$$

3.5. Simulation Results

In this section, simulation results with theoretical analysis are shown for STBC and SM schemes employing dual-polarized 2×1 and 2×2 antenna systems (equivalently 4×2 and 4×4 virtual MIMO system). Different channel conditions are obtained using different receive correlation (r), transmit correlation (t) and spatial correlation (s) coefficients and XPD factors (α) for dual-polarized system under quasi-static Rayleigh fading channel ($K = 0$) conditions, whereas in uni-polarized systems the channel is assumed to be uncorrelated. Signal-to-noise ratio (SNR) is defined as $10\log(2E_s/\sigma_n^2)$ (dB) for uni-polarized systems with two transmit antennas and $10\log(4E_s/\sigma_n^2)$ (dB) for two dual-polarized transmitter antenna systems. Results of Figures 3.3 - 3.6 are summarized in Table 3.1.

Table 3.1. Performance comparison of dual-polarized 2×1 system to uni-polarized 4×2 and 2×1 antennas in dB units.

	$\alpha = 0.9$		$\alpha = 0.5$		$\alpha = 0.2$	
	4×2	2×1	4×2	2×1	4×2	2×1
r, t= 0.1	-0.2	10.5	-1.5	9	-2.5	8
r, t= 0.4	-1	9.8	-2	9	-2.7	7.7
$r = 0.7$ $t = 0.1$	-1	9.8	-2	9	-2.5	7.9
$r = 0.1$ $t = 0.7$	-1	9.8	-2	9	-2.5	7.9

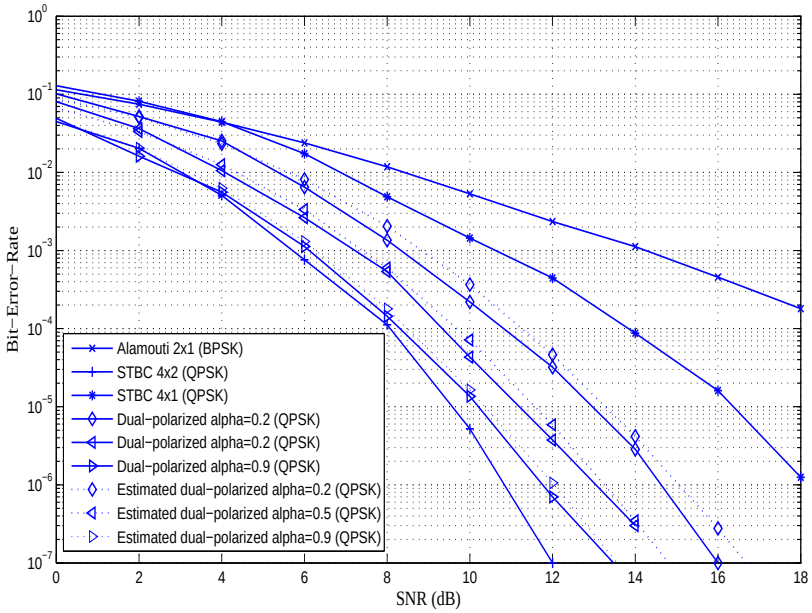

Figure 3.3. Performance analysis of 2x1 dual polarized antennas ($r = 0.1$, $t = 0.1$, $s = 0.05$, $\alpha = 0.2, 0.5, 0.9$)

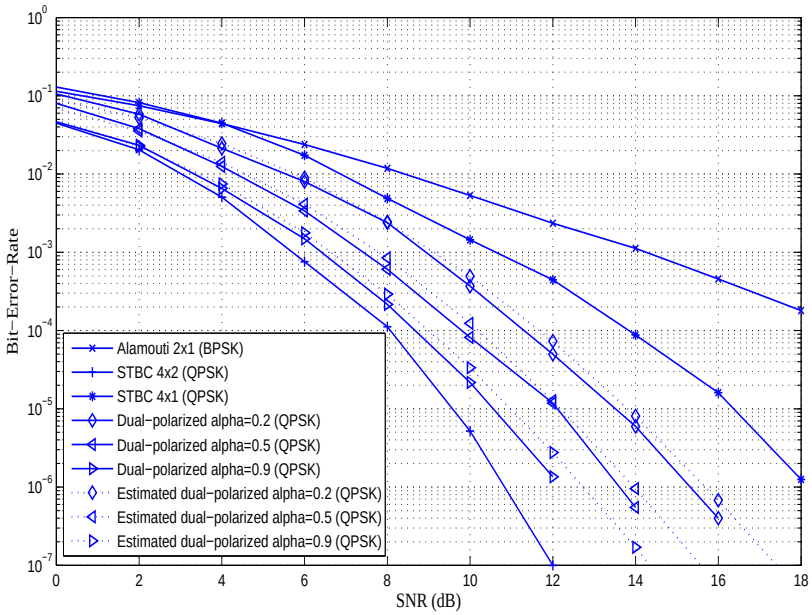

Figure 3.4. Performance analysis of 2x1 dual polarized antennas ($r = 0.4$, $t = 0.4$, $s = 0.05$, $\alpha = 0.2, 0.5, 0.9$)

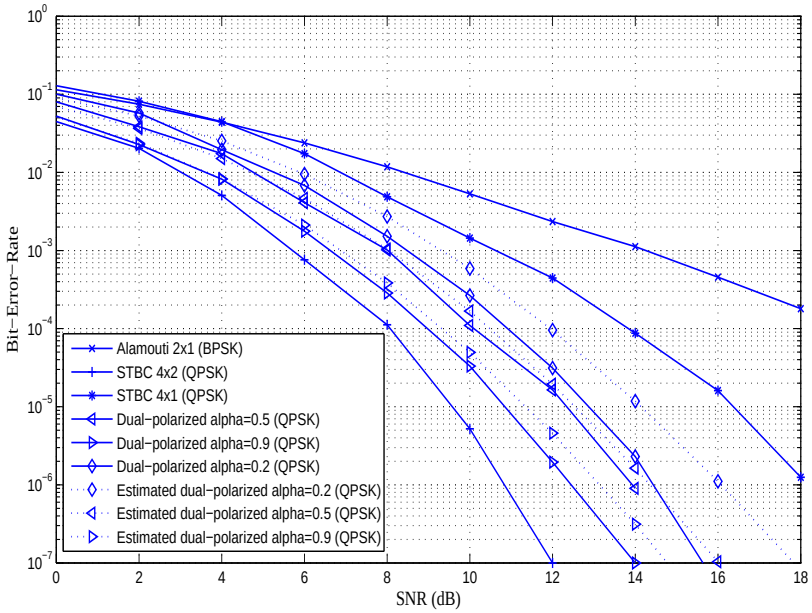

Figure 3.5. Performance analysis of 2x1 dual polarized antennas ($r = 0.7$, $t = 0.1$, $s = 0.05$, $\alpha = 0.2, 0.5, 0.9$)

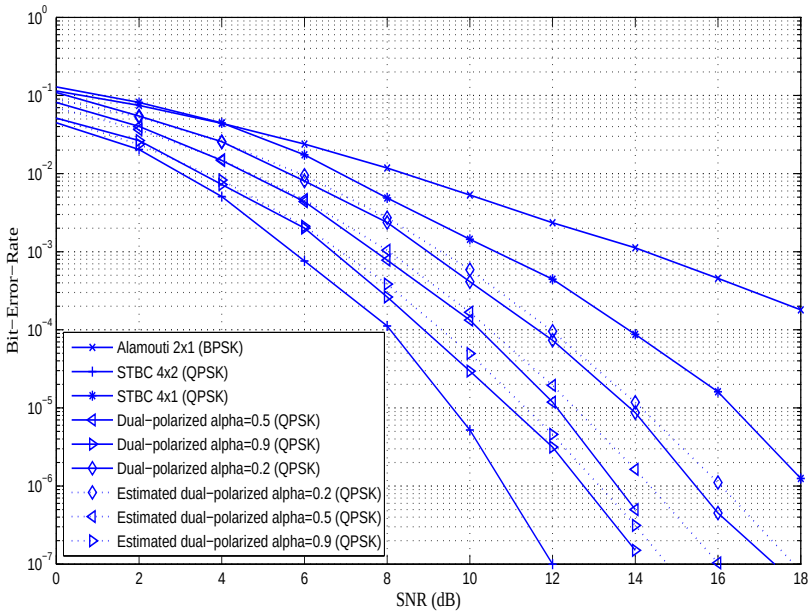

Figure 3.6. Performance analysis of 2x2 dual polarized antennas ($r = 0.1$, $t = 0.7$, $s = 0.05$, $\alpha = 0.2, 0.5, 0.9$)

As also shown in Table 3.1, the system performance decreases about 1 dB with choosing α from 0.9 to 0.5 and 0.5 to 0.2 regardless of the transmit and receive correlations. However, the system performance never decreases beyond Alamouti 2×1 and STBC 4×1 systems with uni-polarized antennas for even high XPD factor and transmit and receive correlations. And in good channel condition where correlation effects and XPD factor are low, the system performance is close to uni-polarized STBC 4×2 system. It is also noted that transmit and receive correlations have the almost same effect on the system performance.

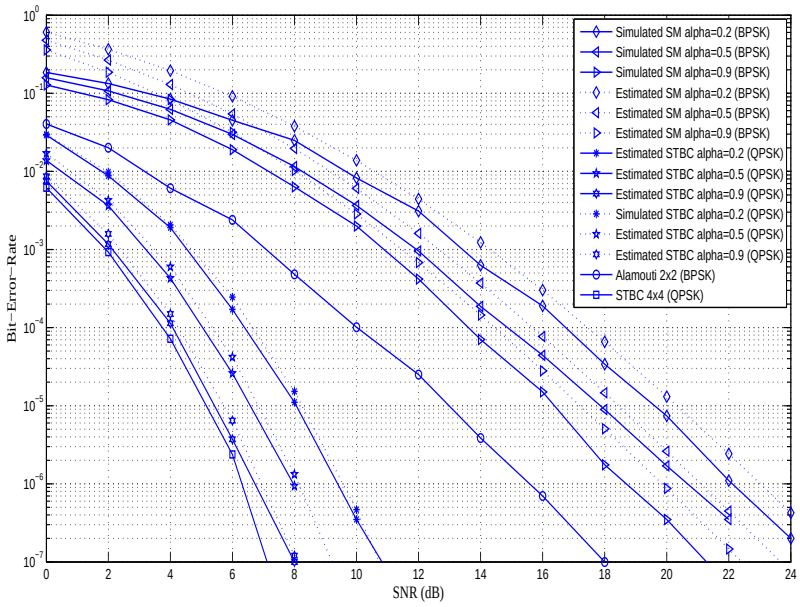

Figure 3.7. Performance of 2x2 dual polarized antennas ($r = 0.1$, $t = 0.1$, $s = 0.05$, $\alpha = 0.2, 0.5, 0.9$)

In Figs. 3.7 - 3.8, the performance of a 2×2 dual-polarized antenna system employing either STBC or SM is shown for a correlated Rayleigh fading channel for dual-polarized and uni-polarized systems, respectively. In low correlations and low XPD factor case (see Fig. 3.7), STBC 2×2 dual-polarized system with QPSK modulation has about 6 dB performance gain over Alamouti 2×2 uni-polarized system with BPSK modulation at 10^{-4} bit-error-rate threshold. In high correlations and high XPD factor case (see Fig. 3.8), the performance gain is about 5 dB and both systems have 1 bps/Hz throughput. In addition, STBC scheme has about 10 dB and 11 dB

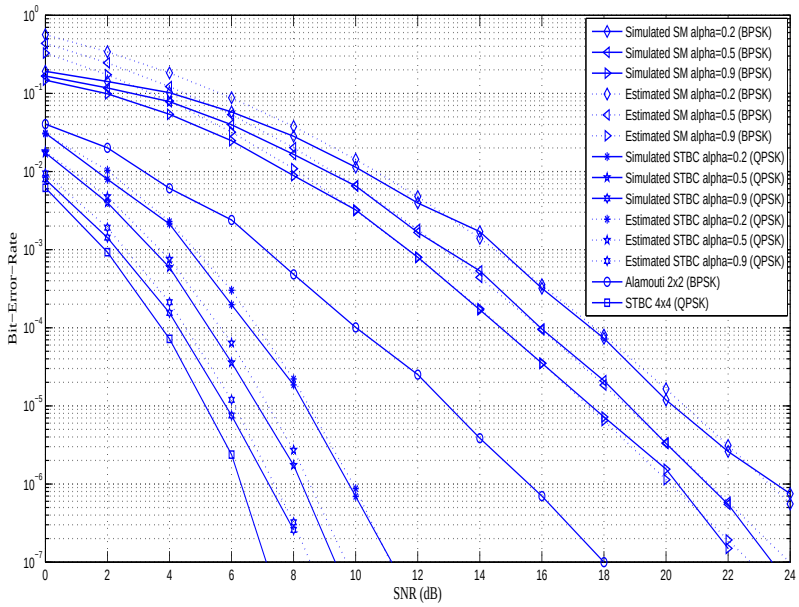

Figure 3.8. Performance of 2x2 dual polarized antennas ($r = 0.4$, $t = 0.4$, $s = 0.05$, $\alpha = 0.2, 0.5, 0.9$)

performance increase over SM scheme at low correlation and high correlation cases, respectively. Moreover, an increase in the correlation coefficients from 0.1 to 0.4 has less than 1 dB effect on the performance. However in high SNR region, SM provides 4 bps/Hz data rate which is four times the data rate of the STBC scheme.

In Fig. 3.9, we simulate the different transmission schemes introduced in this chapter, using QPSK modulation case. Moreover, we show the analytical upper bounds, those of derived in Section 3.2-3.4, together with the simulation results. We also simulate the 1×1 dual-polarized system employing Alamouti and SM which is proposed in [5] for comparison. Notice that analytical results are well in agreement with the simulation results. When considering a 2×2 dual-polarized system STBC provides with approximately 6 dB gain over 2×Alamouti and 9 dB gain over our proposed hybrid transmission scheme (1×SM & 1×Alamouti). On the other hand, STBC provides 1 bps/Hz data rate while 2×Alamouti and our proposed hybrid scheme provides 2 bps/Hz and 3 bps/Hz data rates, respectively. Furthermore, our hybrid scheme has 4 dB advantage over SM which provides a transmission rate of 4 bps/Hz. Thus, a link

adaptation algorithm can fully utilize the channel conditions by switching between those four transmission techniques.

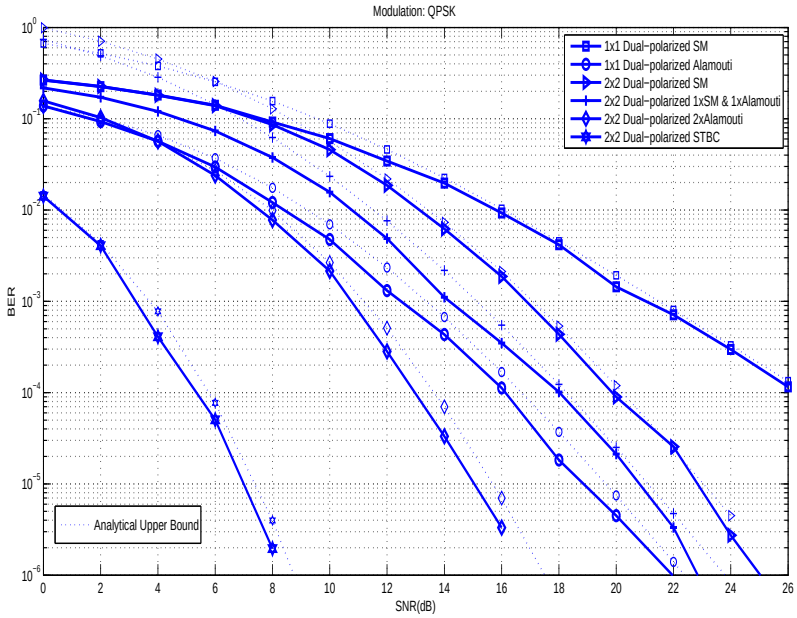

Figure 3.9. Performance of different transmission schemes ($r = 0.3$, $t = 0.5$, $s = 0.05$, $\alpha = 0.4$)

4. SPACE-TIME TURBO EQUALIZATION

Turbo processing techniques have received considerable attention by the discovery of the Turbo codes [32]. In [33], a turbo equalization scheme is proposed for convolutionally coded digital transmission over ISI channels. However computational complexity of this scheme is M^{L_p}; M and L_p being respectively the modulation alphabet size and number of multipaths in the channel. Thus, a low complexity turbo equalization scheme is first appeared in [6] for CDMA systems where multiple access interference (MAI) and ISI are present. Basic principle of this scheme is joint use of SIC and linear MMSE filtering at each iteration step.

In [7], a low complexity iterative receiver is developed for STBC in CDMA systems. While in [8], a low complexity turbo equalization scheme is developed for MIMO communication system where they develop the system for compensating ISI and multiple access interference (MAI) effects of the multi-user communication system, from the results that are derived in [34] for the systems employing receive diversity. Furthermore, many low complexity soft-input soft-output (SISO) equalization algorithms are explored in [9, 10] based on MMSE criterion and in [35] for EDGE systems. Much of these research efforts are performed the equalization in time domain. However, when the channel memory is large, the complexity of the receiver increases due to matrix inversion while calculating MMSE coefficients. On the other hand frequency domain equalizers (FDE) can significantly reduce the complexity using the highly efficient FFT, and have been shown to be an effective solution through [11]-[14]. Equalization can also be employed in frequency domain using OFDM system [15, 16].

In Chapter 3, we showed that the use of dual-polarized antenna elements provides significant performance gain over traditional uni-polarized structures considering same configuration (i.e 2×1 dual-polarized vs 2×1 uni-polarized). On the other hand, although ML detection is optimal solution for suppressing correlation effects and XPD, it brings about tremendous computational load at the receiver especially for SM and hybrid schemes in the case of higher order modulations. Since in next-generation

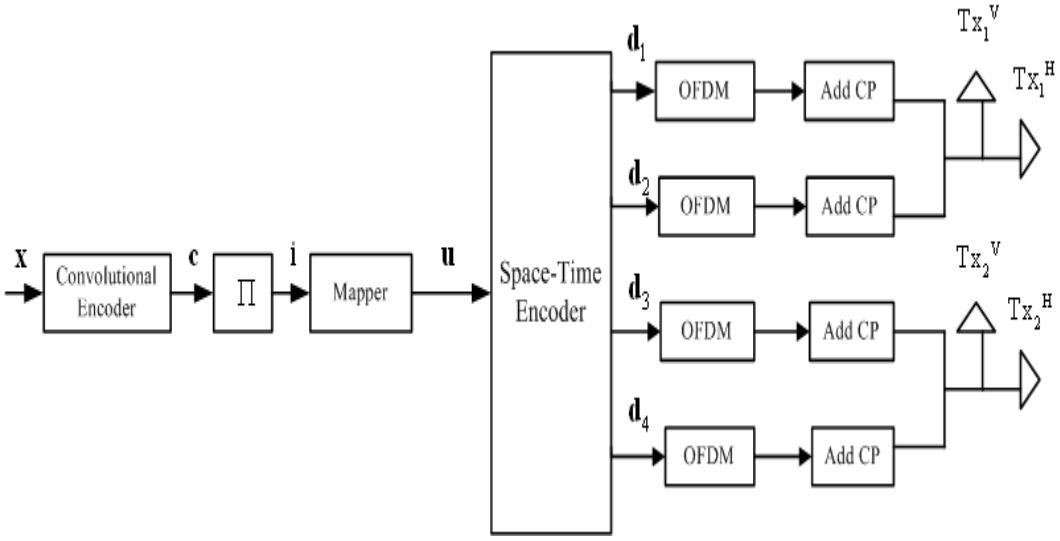

Figure 4.1. Transmitter structure for 2×2 dual-polarized MIMO communication system

wireless communication systems (i.e IEEE 802.11n standard), adaptive modulation and coding is employed, different modulation techniques up to 64-QAM are used. Therefore, it is hard to implement dual-polarized antenna systems with ML decoding, when considering SM and hybrid schemes, in those of high data rate communication systems. In this regard, we proposed a low complexity space-time turbo equalization method for 2×2 dual-polarized systems considering different transmission techniques represented in Chapter 3.

4.1. System Model

The transmitter and the receiver structures of 2×2 dual-polarized antenna system are given in Figure 4.1 and Figure 4.2, respectively.

Information symbols $x_n \in \{0, 1\}$ for $n = 0, 1, ..., N-1$ are first encoded by rate-N_c convolutional encoder to form the coded bits $c_s \in \{-1, 1\}$ for $s = 0, 1, ..., L_c - 1$. And then random bit-wise interleaving operation is employed to form the symbols i_s. Interleaving operation permutes the coded symbol vector $\mathbf{c}$ and is denoted as $\mathbf{i} = \Pi(\mathbf{c})$, where $\Pi(.)$ is a fixed random permutation matrix on L_c elements. And then each bits are partitioned into length-m_0 bits and those m_0 bits are mapped

Table 4.1. Values of r_0 and n_0 for different transmission techniques.

	r_0	n_0
STBC	4	8
2×Alamouti	4	2
1×SM + 1×Alamouti	6	2
SM	4	1

according to the complex constellation set $S \in \{S_0, S_1, ..., S_{M-1}\}$ where M denotes the signal modulation order. The resulting complex symbol sequence with elements u_l for $l = 1, 2, ..., L_M$ is parsed into P blocks of length-r_0, where $L_M = r_0 P$ and in vector form $\mathbf{u} = \begin{bmatrix} u_{r_0 p+1} & u_{r_0 p+2} & \dots & u_{r_0(p+1)} \end{bmatrix}$ for $p = 1, 2, ...P$. Each block $\mathbf{u}$ is then encoded by a rate-r_0/n_0 encoder to form the length-n_0 code symbol blocks $\mathbf{d}_{i,p} = \begin{bmatrix} d_{i,r_0 p+1} & d_{i,r_0 p+2} & \dots & d_{i,r_0(p+1)} \end{bmatrix}$ for $i = 1h, 1v, 2h, 2v$ where subscript nv and nh denotes vertical and horizontal polarization of the nth antenna element, respectively. In the case of STBC transmission mode, we employed the code matrix given in (3.16). The code matrices for hybrid 2×Alamouti and 1×SM + 1×Alamouti transmission techniques are given as $\mathbf{G}_{\mathrm{h1}}$ and $\mathbf{G}_{\mathrm{h2}}$, respectively, in (4.1).

$$\mathbf{G}_{\mathrm{h1}} = \begin{bmatrix} s_1 & s_2 \\ s_3 & s_4 \\ -s_2^* & s_1^* \\ -s_4^* & s_3^* \end{bmatrix}, \quad \mathbf{G}_{\mathrm{h2}} = \begin{bmatrix} s_1 & s_2 \\ s_3 & s_4 \\ -s_2^* & s_1^* \\ s_5 & s_6 \end{bmatrix} \tag{4.1}$$

The values of n_0 and r_0 are given for dual-polarized space-time transmission modes in Table 4.1. Finally each of the antenna element sequences are converted into OFDM symbols by taking Z-point inverse discrete Fourier transform (IDFT) where $Z = n_0 P$. In order to eliminate the ISI, cyclic prefix is appended to the each OFDM frame. The cyclic prefix length should be at least the channel memory length L_p.

Taking into consideration that most indoor wireless communication systems are affected by the multipath fading, the channel between the orthogonal polarizations of

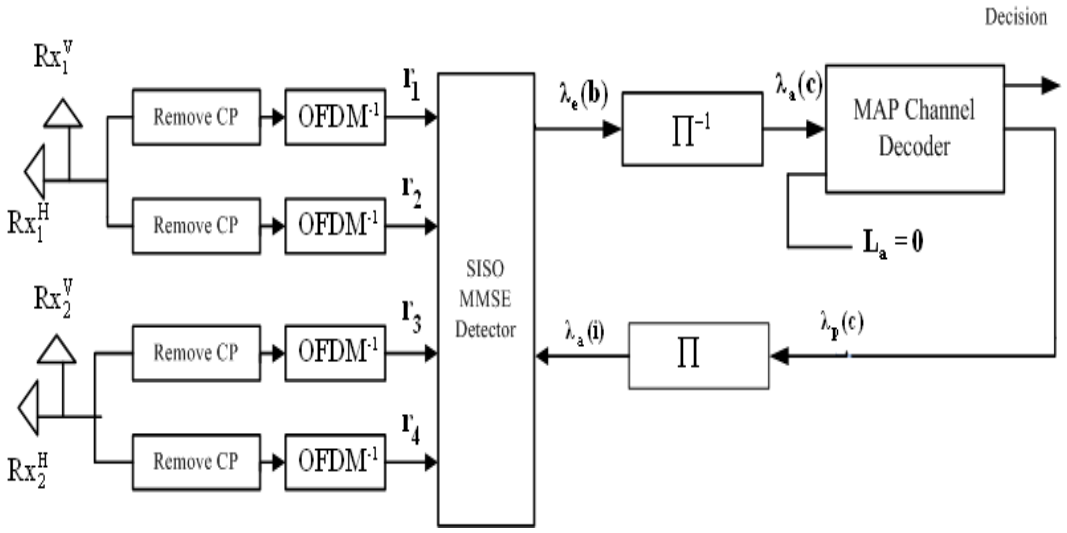

Figure 4.2. Receiver structure for 2×2 dual-polarized MIMO communication system

the transmitter and the receiver antenna elements $h_{j,i}(t)$ is defined as,

$$h_{j,i}(t) = \sum_{l=0}^{L_{p-1}} \alpha_{j,i,l}\delta(t-l) \quad j,i = 1h, 1v, 2h, 2v \tag{4.2}$$

where $\alpha_{j,i,l}$'s are correlated channel coefficients which are obtained from the channel model developed in Chapter 3 for 2×2 dual-polarized MIMO system. $\alpha_{j,i,l}$'s have exponentially decaying power delay spectrum and $\delta()$ represents the Dirac delta function. In the vector form, it can be written as $\mathbf{h}_{j,i} = [\alpha_{j,i,0}, \alpha_{j,i,1}, ..., \alpha_{j,i,L_{p-1}}]$ which is normalized to have unit energy, i.e $\|\mathbf{h}_{j,i}\|^2 = 1$.

After the OFDM demodulation operation, the discrete-time noisy received signal at the jth orthogonal polarization and kth subcarrier can be expressed as,

$$r_{j,k} = \sum_{i=1}^{4} \widehat{h}_{j,i,k} d_{i,k} + n_{j,k} \quad k = 0, 1, ..., Z-1 \tag{4.3}$$

where $\widehat{h}_{j,i,k}$ is the observed channel coefficient which is obtained by Z-point discrete Fourier transform of $\mathbf{h}_{j,i}$ and $n_{j,k}$ is the zero-mean additive white Gaussian noise (AWGN) with variance σ^2. Similarly, $u_{i,k}$ is the kth subband signal from the ith orthogonal polarization.

The signal model in (4.3) can be expressed in terms of space-time encoder input u_l by defining

$$\begin{aligned} \mathbf{r}_{j,k} &= \begin{bmatrix} r_{j,n_0p+1} & r_{j,n_0p+2} & \dots & r_{j,n_0(p+1)} \end{bmatrix} \\ \mathbf{n}_{j,k} &= \begin{bmatrix} n_{j,n_0p+1} & n_{j,n_0p+2} & \dots & n_{j,n_0(p+1)} \end{bmatrix} \end{aligned} \tag{4.4}$$

as the vectors of the received signal and the noise, respectively, for the pth block and jth orthogonal polarization. Then, extending this to the samples for all antennas, the pth receive block can be expressed as

$$\mathbf{r} = \mathbf{H}\mathbf{u} + \mathbf{n} \tag{4.5}$$

where $\mathbf{r} = \begin{bmatrix} \mathbf{r}_1 & \dots & \mathbf{r}_4 \end{bmatrix}^T$ and $\mathbf{n} = \begin{bmatrix} \mathbf{n}_1 & \dots & \mathbf{n}_4 \end{bmatrix}^T$. The structure of $\mathbf{H}$ in the case of SM, STBC and 2×Alamouti and 1×Alamouti + 1×SM transmission techniques are shown below as $\mathbf{H}_{\mathrm{SM}}$, $\mathbf{H}_{\mathrm{STBC}}$, $\mathbf{H}_{\mathrm{h1}}$ and $\mathbf{H}_{\mathrm{h2}}$, respectively.

$$\mathbf{H}_{\mathrm{SM}} = \begin{bmatrix} \widehat{h}_{1h,1h,1} & \widehat{h}_{1h,1v,1} & \widehat{h}_{1h,2h,1} & \widehat{h}_{1h,2v,1} \\ \widehat{h}_{1v,1h,1} & \widehat{h}_{1v,1v,1} & \widehat{h}_{1v,2h,1} & \widehat{h}_{1v,2v,1} \\ \widehat{h}_{2h,1h,1} & \widehat{h}_{2h,1v,1} & \widehat{h}_{2h,2h,1} & \widehat{h}_{2h,2v,1} \\ \widehat{h}_{2v,1h,1} & \widehat{h}_{2v,1v,1} & \widehat{h}_{2v,2h,1} & \widehat{h}_{2v,2v,1} \end{bmatrix}, \tag{4.6}$$

$$\mathbf{H}_{\mathrm{STBC}} = \begin{bmatrix} \widehat{h}_{1h,1h,1} & \widehat{h}_{1h,1v,1} & \widehat{h}_{1h,2h,1} & \widehat{h}_{1h,2v,1} \\ \widehat{h}_{1h,1v,2} & -\widehat{h}_{1h,1h,2} & \widehat{h}_{1h,2v,2} & -\widehat{h}_{1h,2h,2} \\ \widehat{h}_{1h,2h,3} & -\widehat{h}_{1h,2v,3} & -\widehat{h}_{1h,1h,3} & \widehat{h}_{1h,1v,3} \\ \widehat{h}_{1h,2v,4} & \widehat{h}_{1h,2h,4} & -\widehat{h}_{1h,1v,4} & -\widehat{h}_{1h,1h,4} \\ \widehat{h}^{*}_{1h,1h,5} & \widehat{h}^{*}_{1h,1v,5} & \widehat{h}^{*}_{1h,2h,5} & \widehat{h}^{*}_{1h,2v,5} \\ \widehat{h}^{*}_{1h,1v,6} & -\widehat{h}^{*}_{1h,1h,6} & \widehat{h}^{*}_{1h,2v,6} & -\widehat{h}^{*}_{1h,2h,6} \\ \widehat{h}^{*}_{1h,2h,7} & -\widehat{h}^{*}_{1h,2v,7} & -\widehat{h}^{*}_{1h,1h,7} & \widehat{h}^{*}_{1h,1v,7} \\ \widehat{h}^{*}_{1h,2v,8} & \widehat{h}^{*}_{1h,2h,8} & -\widehat{h}^{*}_{1h,1v,8} & -\widehat{h}^{*}_{1h,1h,8} \\ \vdots & \vdots & \vdots & \vdots \\ \widehat{h}_{2v,1h,1} & \widehat{h}_{2v,1v,1} & \widehat{h}_{2v,2h,1} & \widehat{h}_{2v,2v,1} \\ \vdots & \vdots & \vdots & \vdots \\ \widehat{h}^{*}_{2v,2v,8} & \widehat{h}^{*}_{2v,2h,8} & -\widehat{h}^{*}_{2v,1v,8} & -\widehat{h}^{*}_{2v,1h,8} \end{bmatrix}, \tag{4.7}$$

$$\mathbf{H}_{\mathrm{h1}} = \begin{bmatrix} \widehat{h}_{1h,1h,1} & \widehat{h}_{1h,2h,1} & \widehat{h}_{1h,1v,1} & \widehat{h}_{1h,2v,1} \\ \widehat{h}^{*}_{1h,2h,2} & -\widehat{h}^{*}_{1h,1h,2} & \widehat{h}^{*}_{1h,2v,2} & -\widehat{h}^{*}_{1h,1v,2} \\ \vdots & \vdots & \vdots & \vdots \\ \widehat{h}_{2v,1h,1} & \widehat{h}_{2v,2h,1} & \widehat{h}_{2v,1v,1} & \widehat{h}_{2v,2v,1} \\ \widehat{h}^{*}_{2v,2h,2} & -\widehat{h}^{*}_{2v,1h,2} & \widehat{h}^{*}_{2v,2v,2} & -\widehat{h}^{*}_{2v,1v,2} \end{bmatrix}. \tag{4.8}$$

$$\mathbf{H}_{\mathrm{h2}} = \begin{bmatrix} \widehat{h}_{1h,1h,1} & \widehat{h}_{1h,2h,1} & \widehat{h}_{1h,1v,1} & \widehat{h}_{1h,2v,1} & 0 & 0 \\ \widehat{h}^{*}_{1h,2h,2} & -\widehat{h}^{*}_{1h,1h,2} & 0 & 0 & \widehat{h}^{*}_{1h,1v,2} & -\widehat{h}^{*}_{1h,2v,2} \\ \vdots & \vdots & \vdots & \vdots & \vdots & \vdots \\ \widehat{h}_{2v,1h,1} & \widehat{h}_{2v,2h,1} & \widehat{h}_{2v,1v,1} & \widehat{h}_{2v,2v,1} & 0 & 0 \\ \widehat{h}^{*}_{2v,2h,2} & -\widehat{h}^{*}_{2v,1h,2} & 0 & 0 & \widehat{h}^{*}_{2v,1v,2} & -\widehat{h}^{*}_{2v,2v,2} \end{bmatrix} \tag{4.9}$$

4.1.1. SISO MMSE Detector

Using the information provided by the channel decoder, the soft information bits are estimated according to

$$\overline{b}(i_s) = \mathrm{E}\{b(i_s)\} = \tanh\left(\frac{\lambda_a(i_s)}{2}\right) \quad s = 0, 1, ..., N-1 \tag{4.10}$$

where $\lambda_a(i_s)$ is the a priori information which is zero at the first iteration assuming equiprobable bits are transmitted. And then bit-to-symbol mapping is employed for interference cancellation according to

$$\overline{u}_l = \mathrm{E}\{u_l\} = \sum_{\widehat{p}=0}^{M-1} S_{\widehat{p}} P(b_m = S_{\widehat{p}}) \quad m = 1, 2, ..., m_0 \tag{4.11}$$

The variance $\mathrm{VAR}\{u_l\}$ of the symbol u_l on the basis of a priori information is calculated as,

$$\mathrm{VAR}\{u_l\} = \mathrm{E}\{|u_l|^2\} - |\overline{u}_l|^2, \tag{4.12}$$

$$\mathrm{E}\{|u_l|^2\} = \sum_{\widehat{p}=0}^{M-1} |S_{\widehat{p}}|^2 P(b_m = S_{\widehat{p}}). \tag{4.13}$$

If the energy of each symbol is equal, i.e M-PSK, the expression $\mathrm{E}\{|u_l|^2\}$ is constant and equals to σ_s^2 which is the variance of a symbol without a priori information. If the energy of each symbol is not equal, i.e M-QAM, the variance has to be calculated explicitly as in (4.13).

After soft symbol generation, we form soft information in vector form as $\overline{\mathbf{u}}_i = \begin{bmatrix} \overline{u}_1 & \dots & 0 & \dots & \overline{u}_{k_0} \end{bmatrix}$ where the ith element is equal to zero. And then soft interference cancellation (SIC) is employed as

$$\widetilde{\mathbf{r}} = \mathbf{r} - \overline{\mathbf{r}}_i = \mathbf{H}(\mathbf{u} - \overline{\mathbf{u}}_i) + \mathbf{n}. \tag{4.14}$$

Notice that in SIC, only the desired symbol is remained, the interference from the other

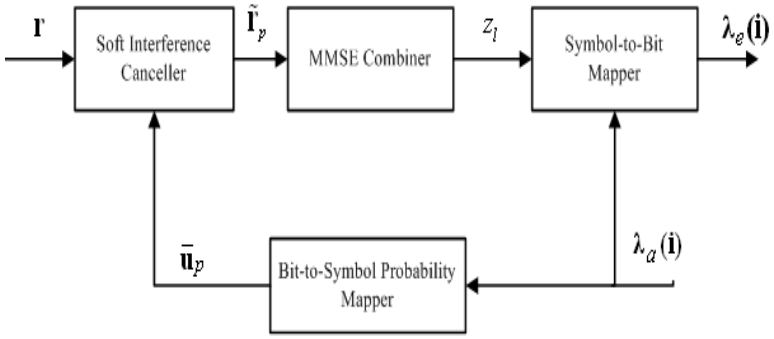

Figure 4.3. Structure of MMSE-FDE based SISO space-time decoder.

symbols cancel out in a soft process, thus the vector $\widetilde{\mathbf{r}}$ is only carrying information about the desired symbol. The output of the MMSE filter is

$$\mathbf{y}_i = \mathbf{w}_i^H \widetilde{\mathbf{r}}_i \tag{4.15}$$

where $\mathbf{w}_i = \Big[w_1, w_2, ..., w_{4n_0}\Big]$ is the MMSE filter coefficient vector which minimizes the mean-squared error between desired symbol and filter output given as

$$\begin{aligned} \mathbf{y}_i &= \text{argmin } \mathrm{E}\{\|u_l - \mathbf{w}_i^H \widetilde{\mathbf{r}}\|\} \\ &= \mathbf{w}_i^H \mathrm{E}\{\widetilde{\mathbf{r}}\widetilde{\mathbf{r}}^H\}\mathbf{w}_i - 2\mathbf{w}_i^H \mathrm{E}\{u_l \widetilde{\mathbf{r}}\}. \end{aligned} \tag{4.16}$$

Taking the gradient with respect to $\mathbf{w}_i$ and setting it to zero to obtain

$$\mathrm{E}\{\widetilde{\mathbf{r}}\widetilde{\mathbf{r}}^H\}\mathbf{w}_i - \mathrm{E}\{u_l \widetilde{\mathbf{r}}\} = 0. \tag{4.17}$$

where

$$\begin{aligned} \mathrm{E}\{\widetilde{\mathbf{r}}\widetilde{\mathbf{r}}^H\} &= \mathrm{E}\Big\{(\mathbf{H}(\mathbf{u} - \overline{\mathbf{u}}_i) + \mathbf{n})(\mathbf{H}(\mathbf{u} - \overline{\mathbf{u}}_i) + \mathbf{n})^H\Big\} \\ &= \mathbf{H}\mathrm{E}\Big\{(\mathbf{u} - \overline{\mathbf{u}}_i)(\mathbf{u} - \overline{\mathbf{u}}_i)^H\Big\}\mathbf{H}^H + \sigma^2 \mathbf{I}_{4n_0} \\ &= \mathbf{H}\Phi_i \mathbf{H}^H + \sigma^2 \mathbf{I}_{4n_0} \end{aligned} \tag{4.18}$$

where σ^2 is variance of the noise and $\Phi_i = \text{diag}\Big\{\text{VAR}\{u_1\}, ..., \sigma_s^2, ..., \text{VAR}\{u_{r_0}\}\Big\}$ in

which the ith element is σ_s^2. $\mathbf{I}_{4n_0}$ refers the $4n_0 \times 4n_0$ identity matrix. Notice that the transmitted symbols are assumed to be uncorrelated and the elements of Φ_i are obtained using

$$E\Big\{(\mathbf{u}-\overline{\mathbf{u}}_i)(\mathbf{u}-\overline{\mathbf{u}}_i)^H\Big\} = \mathrm{E}\{\mathbf{u}\mathbf{u}^H\} - \mathrm{E}\{\mathbf{u}\}\mathrm{E}\{\mathbf{u}\}^H. \tag{4.19}$$

And the second term in (4.17) is calculated as

$$\begin{aligned}\mathrm{E}\{u_l\widetilde{\mathbf{r}}\} &= \mathrm{E}\Big\{u_l(\mathbf{H}(\mathbf{u}-\overline{\mathbf{u}}_i)+\mathbf{n})\Big\} \\ &= \mathbf{H}\mathbf{e}_i \end{aligned} \tag{4.20}$$

where $\mathbf{e}_i$ is all-zero vector except ith element which is equal to 1. Finally, the MMSE coefficients are obtained as,

$$\begin{aligned}\mathbf{w}_i &= E\{u_l\widetilde{\mathbf{r}}\}\Big[E\{\widetilde{\mathbf{r}}\widetilde{\mathbf{r}}^H\}^H\Big]^{-1} \\ &= \Big[\mathbf{H}\Phi_i\mathbf{H}^H + \sigma^2\mathbf{I}_{4n_0}\Big]^{-1}\mathbf{H}\mathbf{e}_i. \end{aligned} \tag{4.21}$$

The extrinsic information can be produced by viewing the combiner output which is produced by an AWGN channel with input u_l as

$$z_l = \phi_l u_l + n_l \tag{4.22}$$

where ϕ_l is the equivalent amplitude of the signal at the filter output, ϕ_l is the channel gain and n_l is complex white gaussian noise and $n_l \sim N(0, \sigma_l^2)$. In order to get the extrinsic information provided by the equalizer, we need to calculate ϕ_l and σ_l^2 which are given in (4.23) and (4.24) (see Apendix A for derivations), respectively.

$$\phi_l = \frac{1}{\varepsilon_{av}}\mathbf{w}_i^H\mathbf{H}\mathbf{e}_i \tag{4.23}$$

$$\sigma_l^2 = (\phi_l - \phi_l^2)\varepsilon_{av} \tag{4.24}$$

ε_{av} denotes the average symbol energy.

4.1.2. Symbol Extrinsic Probabilities Computation

In order to compute the bit extrinsic probabilities, we have first to approximate the symbol extrinsic probabilities. Therefore, we use the Gaussian equivalent channel assumption given in (4.22). Using the parameters ϕ_l and σ_l^2 of the equivalent AWGN channel output is computed for the estimate z_l, the M symbol extrinsic probabilities can be approximated as follows,

$$p(u_{l,m}|z_l) = \frac{1}{\sqrt{2\pi\sigma_l^2}}\exp(-\frac{|z_l - \phi_l u_{l,m}|^2}{2\sigma_l^2}) \qquad m = 0, 1, ..., M-1. \tag{4.25}$$

However, calculating exponential terms may lead to computational errors in the high SNR region, in this regard we define,

$$\widetilde{\kappa}(u_l) = \frac{|z_l - \phi_l u_l|^2}{2\sigma_l^2}. \tag{4.26}$$

for each of the M symbols and compute the bit extrinsic log-likelihood ratios (LLR) in terms of $\widetilde{\kappa}(u_l)$ and the a priori information in the next section.

4.1.3. Bit Extrinsic LLR Computation

A-posteriori probabilities of given coded bits are given as

$$\begin{aligned} \lambda_p(i_{s,m}) &= \log\Big\{\frac{P(i_{s,m}=1)}{P(i_{s,m}=-1)}\Big\} \\ &+ \log\Bigg\{\frac{\sum_{\forall_{u_l}:(i_{s,m}=1)}\exp\Big(\widetilde{\kappa}(u_l) + \sum_{\varrho,q\neq s,m}\frac{1}{2}i_{\varrho,q}\lambda_a(i_{\varrho,q})\Big)}{\sum_{\forall_{u_l}:(i_{s,m}=-1)}\exp\Big(\widetilde{\kappa}(u_l) + \sum_{\varrho,q\neq s,m}\frac{1}{2}i_{\varrho,q}\lambda_a(i_{\varrho,q})\Big)}\Bigg\}. \end{aligned} \tag{4.27}$$

The first term in (4.27) is the a priori information about the symbols $i_{s,m}$ which is also shown as

$$\lambda_a(i_{s,m}) = \log\Big\{\frac{P(i_{s,m}=1)}{P(i_{s,m}=-1)}\Big\} \tag{4.28}$$

The extrinsic bit LLR $\lambda_e(i_{s,m})$, which is the second term in (4.27), can be computed with the max*[.,.] operation [15, 36] as

$$\begin{aligned}\lambda_e(i_{s,m}) &= \max^*_{\forall_{u_l}:(i_{s,m}=1)}\Big[\widetilde{\kappa}(u_l) + \sum_{\varrho,q\neq s,m}\frac{1}{2}i_{\varrho,q}\lambda_a(i_{\varrho,q})\Big] \\ &- \max^*_{\forall_{u_l}:(i_{s,m}=-1)}\Big[\widetilde{\kappa}(u_l) + \sum_{\varrho,q\neq s,m}\frac{1}{2}i_{\varrho,q}\lambda_a(i_{\varrho,q})\Big]\end{aligned} \tag{4.29}$$

where max*[.,.] operation is defined as

$$\max^*[x,y] = \max[x,y] + \log(1+e^{-|x-y|}). \tag{4.30}$$

There is only a slight performance degradation using the MAX-LOG-MAP algorithm, i.e 0.35 dB [37], in Turbo processing. However, using LOG-MAP algorithm requires an additional read-only memory (ROM) which outputs the correction term (second term in (4.30)) [36]. In order to decrease the complexity of the system, we left out the correction term in the simulations.

Finally, the extrinsic information produced by the output of the symbol-to-bit mapper is sent to the channel decoder which is implemented by Bahl, Cocke, Jelinek, and Raviv [38] and referred as BCJR algorithm in turbo processing literature.

Note that in contrast the common practice we feedback the entire a posteriori information from the channel decoder output. In contrast to common practice, we feedback the entire a posteriori information from the channel decoder output since we notice that there is a significant performance degradation when feeding only the extrinsic information in the case of higher order modulations. The same observation is also expressed in [35]. Due to that reason, in simulations throughout the Chapter 5,

we used the whole a posteriori information from channel decoder to SIC process.

4.2. Complexity Analysis

The complexity analysis of ML decoder, introduced in Chapter 3, and iterative SIC/MMSE decoder are given in Table 4.2 in the case of dual-polarized SM and hybrid schemes considering only one block of symbol vector. The abbreviations ADD, MUL, and INV are stand for addition, multiplication, and inverse operations, respectively. In addition, MAX and MIN operations are used to denote finding the maximum and the minimum element in an array, respectively. Note that, the complexity of dual-polarized STBC is less than the value shown in Table 4.2, due to the presence of combining operation before ML decoding. While computing the complexity of dual-polarized STBC, the multiplier M^{2N_t} has to be replaced with M for both ADD and MUL operation. Notice that the decoding and the demodulation operations are separately done at ML receivers, but in iterative system it is a joint operation. However we did not take into account the complexity of the demodulation for ML receivers, since its complexity is negligible as compared to decoder. Main complexity for ML decoders come from the equations (3.23) and (3.32) that are shown for SM and hybrid structures, respectively. We also ignored the complexity of bit-to-symbol mapping operation in which the additional complexity for 2nd and other iterations is introduced.

Table 4.2. Complexity analysis of iterative SIC/MMSE and ML decoders for one data block.

	Iterative SIC/MMSE Decoder	ML Decoder
MUL	$N_{ite}(M \cdot A + 2N_r n_0 \cdot B)r_0$	$(r_0(N_r+1)+1)M^{r_0}$
ADD	$N_{ite}(C + 2N_r n_0 \cdot D)r_0$	$((r_0-1)2N_r + r_0 - 1)M^{r_0}$
INV	$N_{ite} r_0$	-
MAX	$N_{ite} M r_0$	-
MIN	-	1

$$
\begin{aligned}
A &= 5 + ((m_0 - 1) + 1)m_0, \\
B &= r_0 + (r_0/2)^2 + 2N_r n_0 r_0 + 4N_r n_0 + 1, \\
C &= M(m_0 + 3) + m_0 + 1 + r_0, \\
D &= r_0^2 - 1 + 2r_0 N_r n_0.
\end{aligned}
$$

For example, we consider the 2×2 dual-polarized system employing SM scheme for BPSK ($M = 2$, $m_0 = 1$), QPSK ($M = 4$, $m_0 = 2$), 16-QAM ($M = 16$, $m_0 = 4$) and 64-QAM ($M = 64$, $m_0 = 6$) for 4 iterations. The results are pointed out in Table 4.3. Notice that, the complexity of ML decoding increase significantly with respect to modulation order for a fixed number of transmitter antenna elements.

4.3. Simulation Results

In this section, we show the performance results of the different dual-polarized antenna schemes that we introduce in Chapter 3. Throughout the simulations, correlation parameters and the XPD factor are defined as, $r = 0.3$, $t = 0.5$, $s = 0.05$ and $\alpha = 0.4$. In these simulations, we consider the Rayleigh fading channel with 5-taps and employ QPSK modulation and rate-1/2 convolutional encoder with gener-

Table 4.3. Complexity of SIC/MMSE and ML decoders for different modulation techniques in the case of 2×2 dual-polarized system employing SM.

	Iterative SIC/MMSE	ML
BPSK	4.560	449
QPSK	5.184	7.169
16-QAM	11.680	1.835.009
64-QAM	56.512	469.762.049

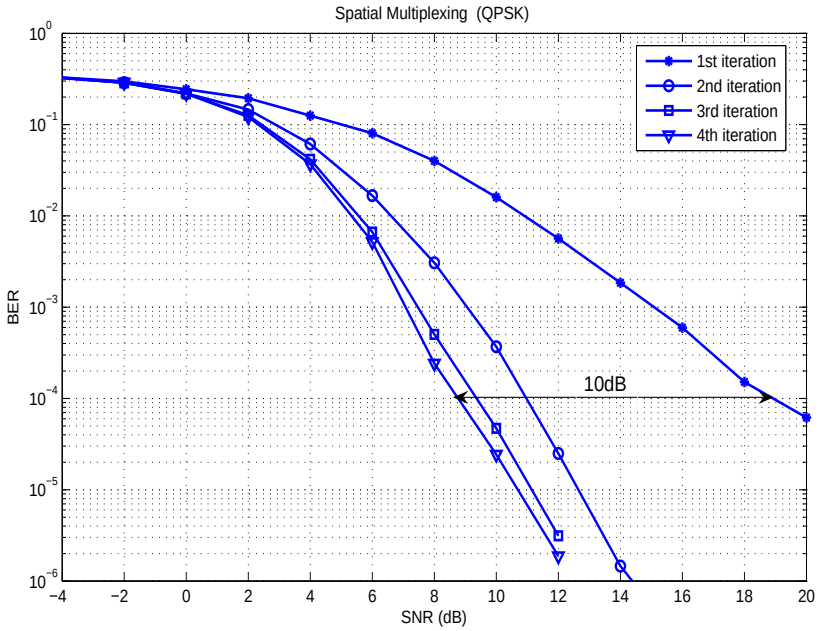

Figure 4.4. Performance of iterative 2×2 dual-polarized system employing spatial multiplexing ($r = 0.3$, $t = 0.5$, $s = 0.05$, $\alpha = 0.4$).

ator $(133, 171)_8$ in octal representation. Throughout the simulations, the channel is assumed to be perfectly estimated at the receiver. The cyclic prefix length is set to five symbols so that ISI effects are avoided. In addition, OFDM size is set to 512. SNR is defined as $10\log 2E_s/\sigma^2$ (dB) since we send four information symbols from the orthogonal polarizations at the same time.

Simulation-1: In the first simulation, we employ spatial multiplexing scheme through orthogonal polarizations of each dual-polarized antenna. As it is also seen from Figure 4.4, the performance of the system increases significantly from 1st iteration to 4th iteration. There is approximately 10 dB performance gain at 10^{-4} BER threshold from 1st the last iteration. During the simulations, we see that there is not any considerable performance increase after four iterations. Furthermore, notice that the complexity of the system increases as we increase the iteration number. In this regard, we can even decrease the iteration number to two where we get about 7dB performance over first iteration according to a performance and complexity trade-off.

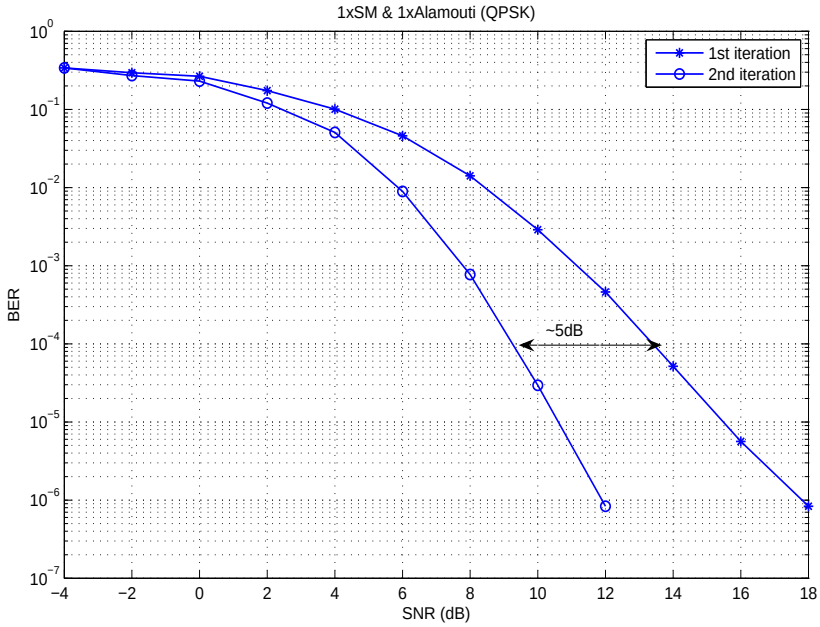

Figure 4.5. Performance of iterative 2×2 dual-polarized system employing hybrid $1\times$SM & $1\times$Alamouti scheme ($r = 0.3$, $t = 0.5$, $s = 0.05$, $\alpha = 0.4$).

Simulation-2: In the second simulation, we employ our proposed hybrid scheme ($1\times$ SM & 1×1 Alamouti) for dual-polarized antenna systems. As shown in Figure 4.5, the performance increase with respect to number of iterations is decreased as compared to spatial multiplexing. Even after the second iteration, we observed that there is not any additional performance gain over second iteration. This may due to the additional diversity resulting from the Alamouti scheme which we send through vertical polarizations of dual-polarized antenna elements. However we get over 5dB performance gain at 10^{-4} BER threshold from first to second iterations.

Simulation-3: Performance of hybrid $2\times$Alamouti scheme is analyzed in the third simulation. This scheme provides 2 dB performance improvement from 1st to 2nd iteration at 10^{-4} BER threshold. Notice in here, two Alamouti blocks are transmitted from each dual-polarized antennas, thus diversity of the system increases in comparison to hybrid $1\times$SM & $1\times$Alamouti scheme. Therefore, the system approaches to getting the best performance at the first iteration.

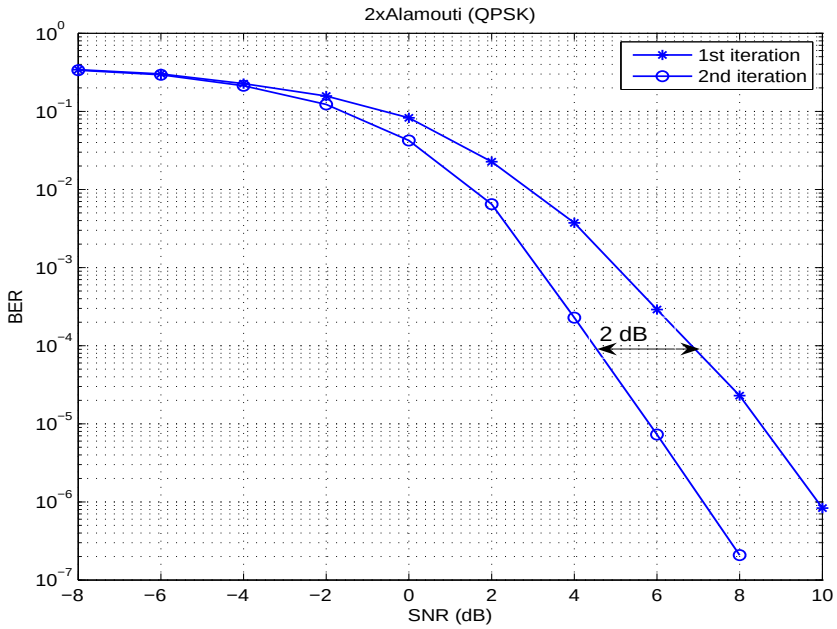

Figure 4.6. Performance of iterative 2×2 dual-polarized system employing hybrid $2\times$ Alamouti scheme ($r = 0.3$, $t = 0.5$, $s = 0.05$, $\alpha = 0.4$).

Simulation-4: In fourth simulation, we employ G_4 STBC coding structure given in [2] to the orthogonal polarizations of dual-polarized MIMO system. In this scheme, very little performance improvement regarding to the iterative process is obtained from first to second iterations. Notice that, we employ 2-dual polarized antenna elements at the transmitter and the receiver. As it is also explained in Chapter 3, a virtual 4×4 MIMO scheme is obtained. Regarding the number of transmit and receive antenna elements of this virtual MIMO scheme, the diversity order of the system is very high, i.e 16. In this respect, this virtual 4×4 STBC scheme with iterative process at the receiver do not provide performance improvement by iterations since it gets very close to the performance that it can achieve.

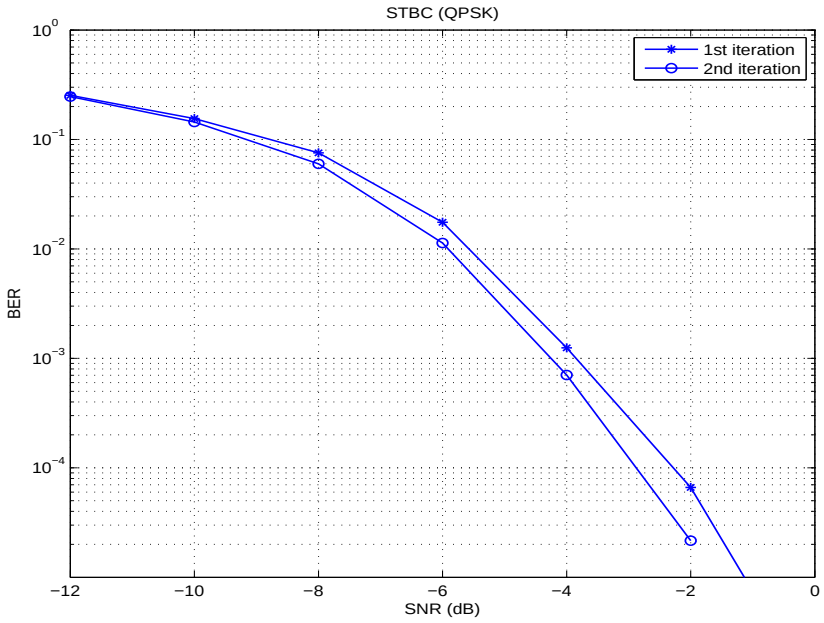

Figure 4.7. Performance of iterative 2×2 dual-polarized system employing G_4 [2] STBC scheme ($r = 0.3$, $t = 0.5$, $s = 0.05$, $\alpha = 0.4$).

5. LINK ADAPTATION

Link adaptation is the way to adapt transmission parameters to the current channel conditions by means of transmission modes. For instance, if the channel conditions are not good (low SNR), the low level transmission modes with lower data rates are employed to have better overall throughput. The general principles of link adaptation algorithms are [39]

- defining a channel quality indicator, that provides some knowledge about the transmission channel and
- adjusting a number of signal transmission parameters to the variations of that indicator over the signaling period.

In some works, the channel quality indicator is determined by the successful and unsuccessful transmissions. For instance, in automatic rate fallback (ARF) [40] algorithm, where it is the first published algorithm that uses such a technique, after ten consecutive successful transmissions, the next higher modulation and coding level is employed while after two consecutive unsuccessful transmissions, next lower modulation and coding level is employed. One of the main advantage of this scheme is that there is no need to have a channel knowledge (i.e channel matrix) at the transmitter. However since ARF algorithm always tries to send the data at higher physical data rates after ten consecutive successful transmissions, in stable systems, this would lead transmission errors. In this regard, adaptive ARF (AARF) algorithm is proposed in [41]. Furthermore, ARF algorithm does not have an ability to separate collision errors from the those due to channel conditions, for that reason, in [42] a collision aware rate adaptation (CARA) algorithm is proposed. On the other hand, in [17] the channel quality indicator is defined as the SNR knowledge where the receiver can obtain after each transmission according to the received signal strength and the noise floor.

Recall that in Chapter 3, we introduce transmission techniques together with analytical expressions for dual-polarized antenna systems. We also noted that it is not

feasible to implement this system since the complexity of the ML receivers increases exponentially by the number of information streams transmitted at the unit time from the antennas and the modulation size. In this regard, we propose a space-time turbo equalization technique for dual-polarized systems as a lower complexity alternative in Chapter 4. Remember that, by changing only the channel matrix, the proposed receiver can detect the symbols for different dual-polarized MIMO options.

In this chapter, we employ the link adaptation algorithm in [17], to the dual-polarized system introduced in Chapter 4 for IEEE 802.11n links. Together with modulation and coding schemes (MCS) using in IEEE 802.11n standard, the dual-polarized MIMO schemes that is introduced in former chapters, the transmission channel can be fully utilized via this link adaptation algorithm. In this chapter, we also show the performance and range improvement over conventional 802.11n system.

5.1. IEEE 802.11n Standard

Wireless local area networks (WLAN) are evolving towards the development of broadband applications, i.e IPTV or VOIP, in a way to compete with the wired LAN systems. It is expected that the rapid growth of mobile users will demand the development of new applications with broadband access and bit rates higher than 54 mbps that is currently offered by the IEEE 802.11a and g standards. In this regard, in the development process of the IEEE 802.11n it is aimed to provide higher throughput and higher transmission range with an increased reliability in order to offer similar types of service to its wired counterpart. Therefore, some enhancements in physical (PHY) and medium access control (MAC) layers are included in the IEEE 802.11n standard in comparison to current IEEE 802.11 standards. The basic enhancements in PHY layer can be summarized as follows:

- The use of multiple transmitter and receiver antennas (MIMO)is the key enhancement in PHY layer. The system allows to use SM and STBC to offer higher data rates and reliability, respectively. Data rates that are achieved by using different MCS's and MIMO transmission modes are given in Table 5.1 for 40 Mhz band-

width and long guard interval case. Notice that there are 8 MCS for each MIMO scheme.

- Channel bonding (i.e, use of two 20 Mhz bandwidth streams).This technique allows to use either 20 Mhz or 40 Mhz signalling bandwidth. If 20 Mhz bandwidth is used, data rates would be the half the rates shown in Table 5.1.
- Advanced channel coding, such as low density parity check codes (LDPC). However this coding technique is left optional in the standard. 802.11 systems use convolutional coding with given code rates in Table 5.1.

Basic modifications to the MAC include the addition of frame aggregation which is basically to send the multiple MAC frames into one PHY layer to reduce overhead. With frame aggregation MAC layer throughput can be increased to 100 Mbps. Furthermore, in order to further reduce the overhead, block acknowledgement mechanism is used. In block acknowledgement (ACK) procedure, multiple frames are acknowledged in a single ACK frame.

5.2. Link Adaptation For 802.11n Using Dual-Polarized Antenna Elements

Throughput of the system can be maximized through the use of highest modes that best performs in the given channel conditions. On the other hand, real-time applications, such as voice and video, are very sensitive to delay and jitter. In such systems, running below a certain BER threshold would reduce the number of retransmissions at the upper layers. This would help to avoid buffer overflows and increase the quality of service for these applications. In this regard, a good link adaptation algorithm should also consider a bit-error-rate (BER) threshold and stay behind this threshold at runtime. Simply, if the packet error rate threshold is set to 10^{-1} at PHY layer, with seven retransmissions at the MAC layer, the packet error rate at the network layer would be about 10^{-7}. With such a low packet error probability, there would not be any problem during the streaming. Considering the real-time applications, we set a BER threshold of 10^{-5} for the link adaptation. However different targets may be chosen depending on

Table 5.1. IEEE 802.11n PHY data rates for different MCS's and MIMO modes in the case of 40 Mhz bandwidth and long guard interval [43].

MCS Index	Modulation	Coding Rate	MIMO Mode	Data Rate
0	BPSK	1/2	STBC	13.5 Mbps
1	QPSK	1/2	STBC	27 Mbps
2	QPSK	3/4	STBC	40.5 Mbps
3	16-QAM	1/2	STBC	54 Mbps
4	16-QAM	3/4	STBC	81 Mbps
5	64-QAM	2/3	STBC	108 Mbps
6	64-QAM	3/4	STBC	121.5 Mbps
7	64-QAM	5/6	STBC	135 Mbps
8	BPSK	1/2	SM	27 Mbps
9	QPSK	1/2	SM	54 Mbps
10	QPSK	3/4	SM	81 Mbps
11	16-QAM	1/2	SM	108 Mbps
12	16-QAM	3/4	SM	162 Mbps
13	64-QAM	2/3	SM	216 Mbps
14	64-QAM	3/4	SM	243 Mbps
15	64-QAM	5/6	SM	270 Mbps

the system. For a given BER, packet error rate at the PHY level is calculated as

$$P_p = 1 - (1 - P_b)^{length} \tag{5.1}$$

where P_b indicates the BER. In our simulations, the packet length is assumed to 1000 byte at the PHY level.

Recall that in the former chapters, we introduce 4 transmission techniques for dual-polarized systems, namely 2×Alamouti, 1×SM & 1×Alamouti, 2×2 STBC and 2×2 SM where each one have different spectral efficiency. In Figures 5.1-5.4, we show the performance of these transmission techniques as a function of the SNR for MCS's

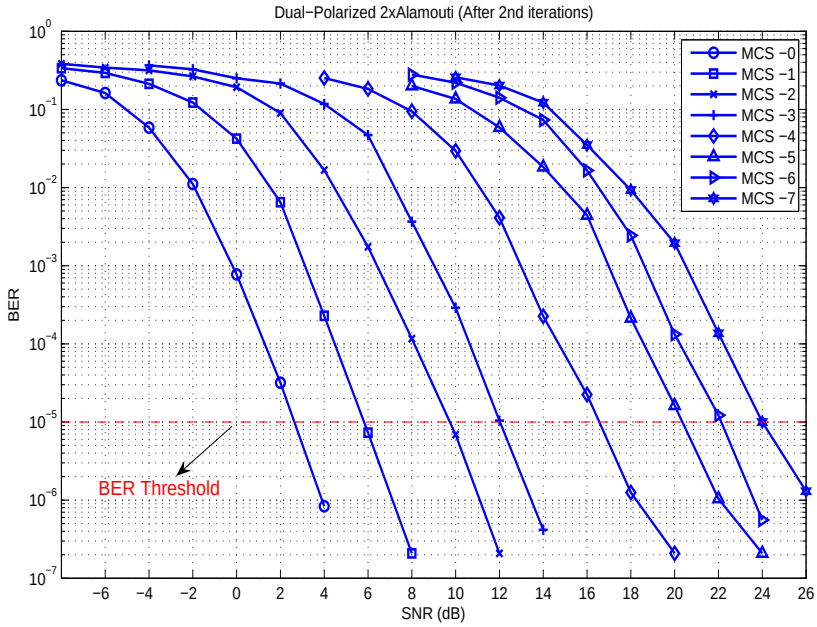

Figure 5.1. Performance of iterative 2×2 dual-polarized system employing $2\times$Alamouti scheme through MCS-0 to MCS-7 ($r = 0.3$, $t = 0.5$, $s = 0.05$, $\alpha = 0.4$).

defined in the standard. We also show the performance of 1×1 dual-polarized Alamouti and SM schemes in Figure 5.5 and Figure 5.6 for comparison. We use the iterative receiver structure introduced in Chapter 4, since it is a lower complexity alternative to ML decoder introduced in Chapter 3. Together with the modulation and coding schemes defined in IEEE 802.11n standard, it is possible to achieve higher PHY level throughput, up to 600 Mbps in the case of short guard interval. In the following simulations, we show the performance of the dual-polarized transmission schemes for MCS's defined in the IEEE 802.11n standard.

Throughout the simulations, correlation parameters and the XPD factor are defined as $r = 0.3$, $t = 0.5$, $s = 0.05$ and $\alpha = 0.4$. And we consider only the NLOS situations with 7-taps and employ convolutional encoder with generator $(133, 171)_8$ in octal representation as it is also defined for the standard. Furthermore, with respect to standard OFDM size is set to 512.

It is easily seen that for a fixed channel conditions, each transmission modes

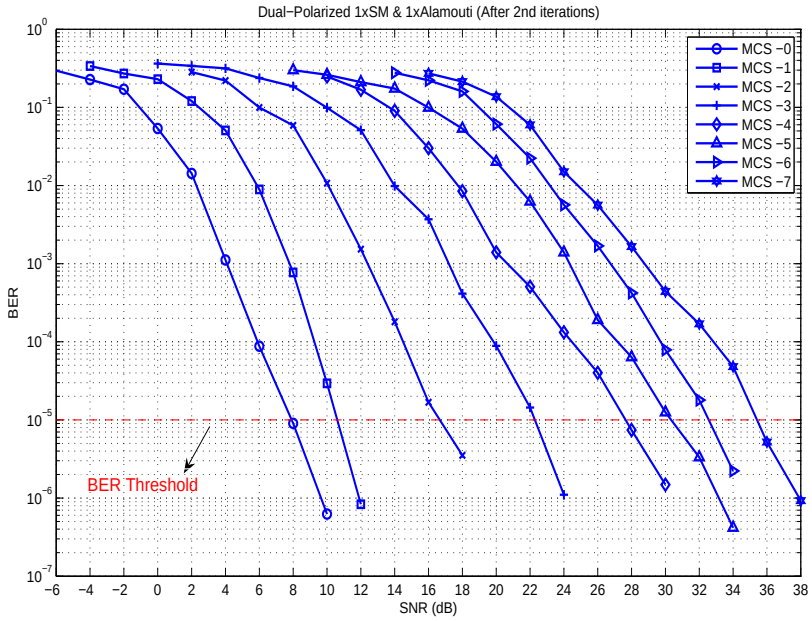

Figure 5.2. Performance of iterative 2×2 dual-polarized system employing 1×SM & 1×Alamouti scheme through MCS-0 to MCS-7 ($r = 0.3$, $t = 0.5$, $s = 0.05$, $\alpha = 0.4$).

require a minimum value of SNR in order to satisfy a predefined target BER. Note that, the SNR thresholds can vary for the different channel conditions where we only consider Rayleigh fading case.

The combination of four dual-polarized MIMO schemes and with eight MCSs results in a total of 32 different transmission modes from which we select a subset of 12 modes as shown in Figure 5.7. These modes maximize the PHY level throughput at certain target BER. In the link adaptation algorithm for dual-polarized MIMO system, we define the SNR as a channel quality indicator, and build a look-up table that conveys the SNR knowledge into the error performance. Optimal transmission mode, that maximizes the throughput for a predefined target BER, is adaptively chosen depending on the current channel condition. As soon as the proper mode selection is done at the receiver, this information is conveyed to the transmitter through a low rate feedback channel. The look-up table is obtained according to the Figure 5.7 and given in Table 5.2. Notice that, our proposed hybrid scheme provides significant throughput improvement between 4 dB-16 dB and 20 dB-26 dB. On the other hand, 2×Alamouti

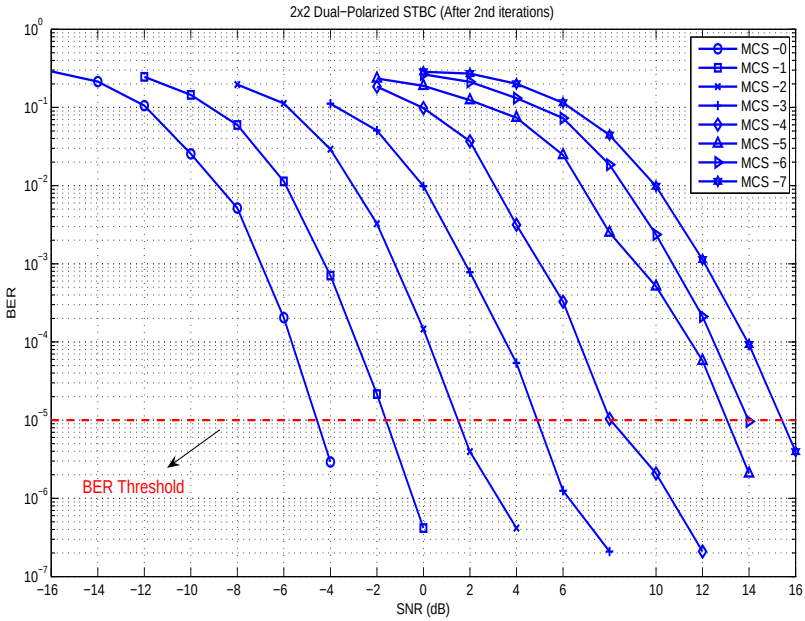

Figure 5.3. Performance of iterative 2×2 dual-polarized system employing G_4 [2] STBC scheme through MCS-0 to MCS-7 ($r = 0.3$, $t = 0.5$, $s = 0.05$, $\alpha = 0.4$).

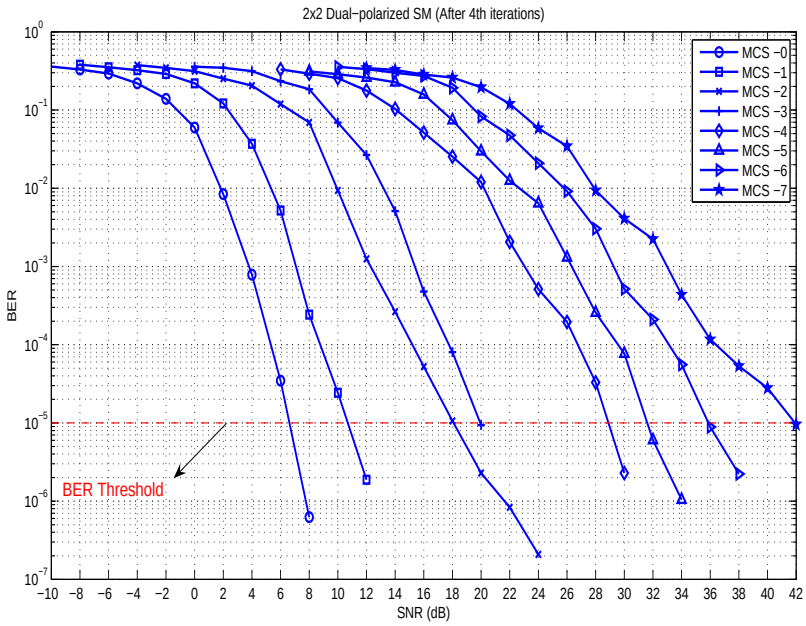

Figure 5.4. Performance of iterative 2×2 dual-polarized system employing SM scheme through MCS-0 to MCS-7 ($r = 0.3$, $t = 0.5$, $s = 0.05$, $\alpha = 0.4$).

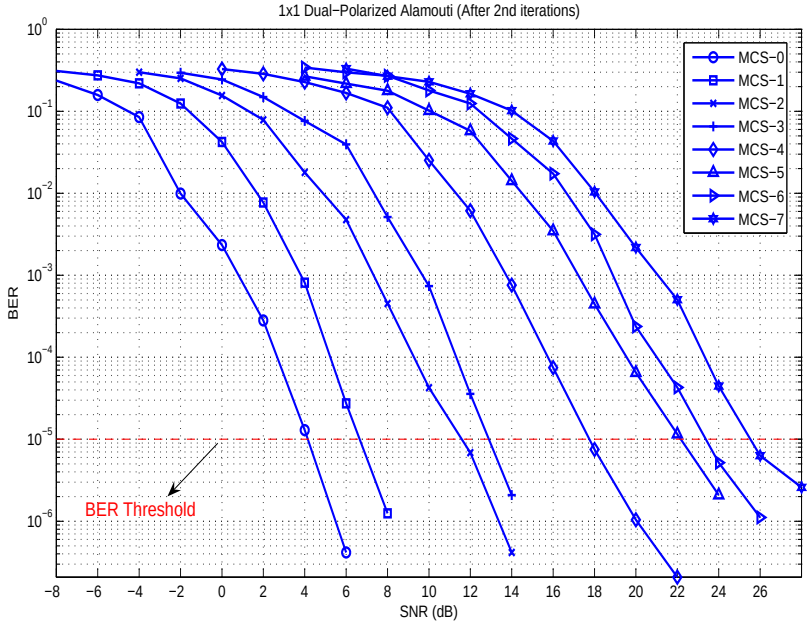

Figure 5.5. Performance of iterative 1×1 dual-polarized system employing Alamouti scheme through MCS-0 to MCS-7 ($r = 0.3$, $t = 0.5$, $s = 0.05$, $\alpha = 0.4$).

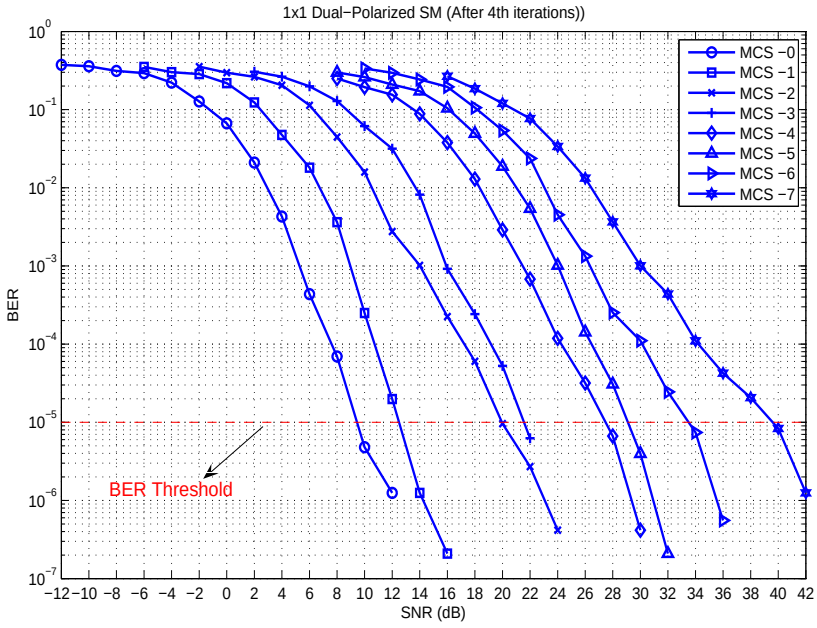

Figure 5.6. Performance of iterative 1×1 dual-polarized system employing SM scheme through MCS-0 to MCS-7 ($r = 0.3$, $t = 0.5$, $s = 0.05$, $\alpha = 0.4$).

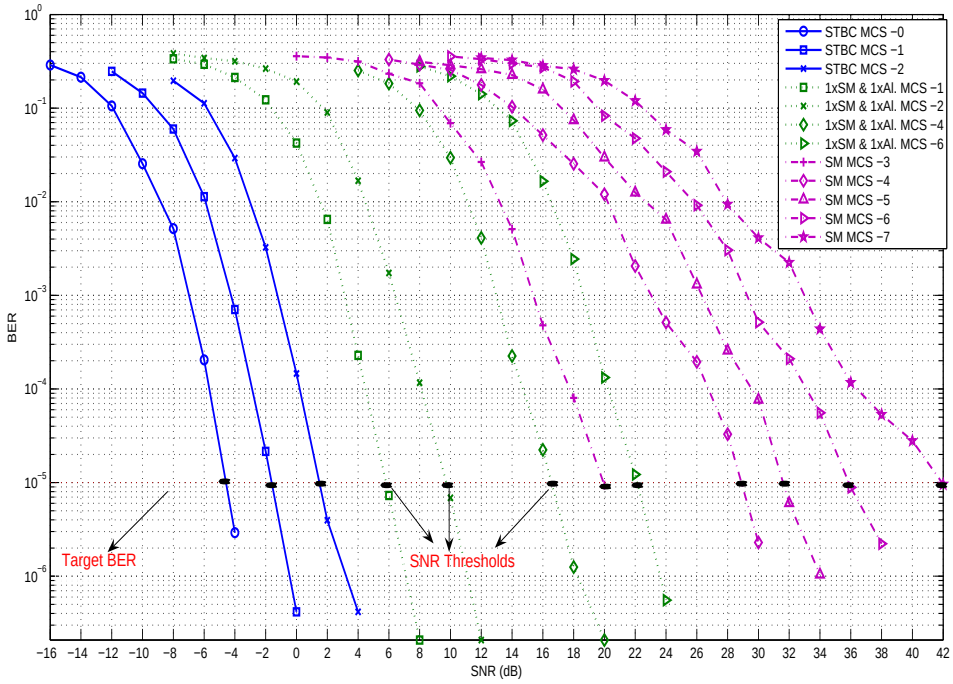

Figure 5.7. Optimum modes to provide best throughput below 10^{-5} BER threshold.

do not provide any additional throughput increase for the whole system. But we only consider the 802.11n links as an example.

In Figure 5.8, PHY level throughput of the adaptive algorithm is shown for 2×2 dual-polarized MIMO system using MCS's defined in IEEE 802.11n system. A throughput analysis of the conventional uni-polarized IEEE 802.11n system is also given in the same figure. For a fair comparison, iterative MMSE equalization is used at the receiver for both uni-polarized and dual-polarized 802.11n systems. We also assume that, there is enough spatial distance between uni-polarized antennas of conventional 802.11n system and scattering properties of the environment do not introduce any correlation between parallel channels. According to the simulation results, the use of dual-polarized antennas provide a double throughput and a significant coverage increase.

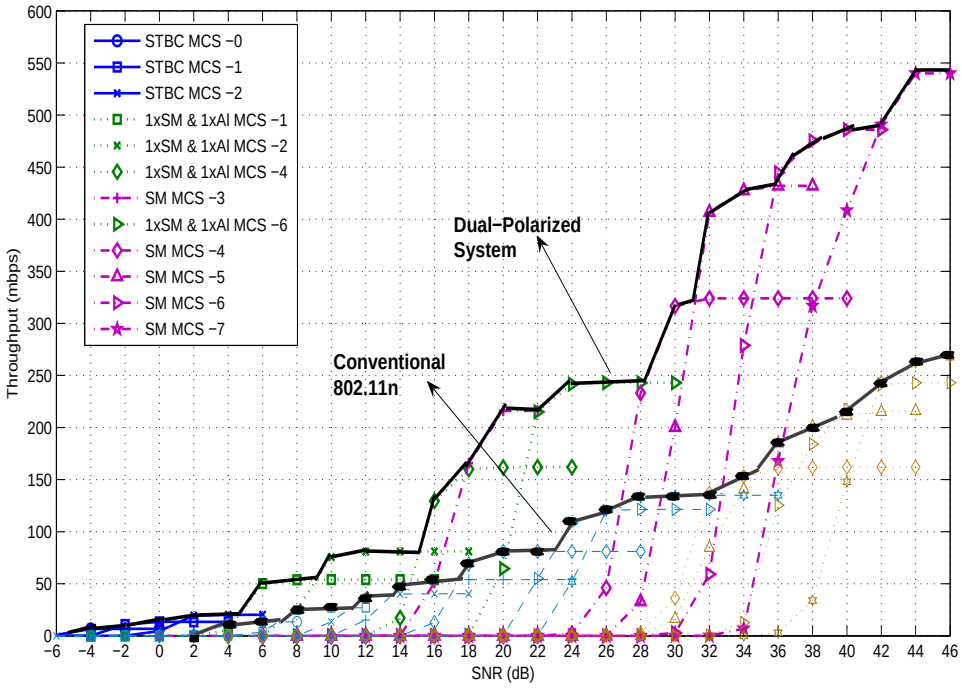

Figure 5.8. PHY level throughput of our link adaptation algorithm.

Table 5.2. Look-up table.

SNR Interval	Transmission Mode
-5dB - -1.8dB	STBC MCS -0
-1.8dB - 1.8dB	STBC MCS -1
1.8dB - 5.8dB	STBC MCS -2
5.8dB - 9.8dB	1×SM & 1×Alamouti MCS -1
9.8dB - 16.5dB	1×SM & 1×Alamouti MCS -2
16.5dB - 20dB	1×SM & 1×Alamouti MCS -4
20dB - 22dB	SM MCS -3
22dB - 29dB	1×SM & 1×Alamouti MCS -6
29dB - 31.5dB	SM MCS -4
31.5dB - 36dB	SM MCS -5
36dB - 42dB	SM MCS -6
42dB <	SM MCS -7

6. CONCLUSIONS

In this thesis, the performance of multiple dual-polarized antenna elements are evaluated for SM and STBC via both theoretical analysis and simulation results. In both scenarios, the use of dual-polarized antennas provide a significant performance improvement over the use of uni-polarized antenna elements. In addition, we also proposed a new hybrid scheme, and analyzed this new scheme together with an other hybrid structure studied in the literature for dual-polarized MIMO systems. It was shown that, a transmission channel can be fully utilized switching between these transmission techniques.

In the analysis of SM and hybrid structures, we employed ML decoder since it provides better performance than ZF and MMSE receivers. However, the complexity of the ML decoding increases with the modulation size for a fixed MIMO configuration although it is an optimal solution to suppress correlation effects and XPD factor. In this regard, we changed our way to the low complexity iterative receiver structures where we could get closer to the performance of ML decoding in an iterative fashion. Throughout the simulations, we achieved remarkable performance improvement from first to other iterations for SM and hybrid schemes.

In combination of four transmission techniques with modulation and coding schemes, we got increased number of transmission parameters to adopt the channel conditions. Using these signalling parameters we employ a standard link adaptation algorithm that defines SNR knowledge as channel quality indicator. As an example, we consider IEEE 802.11n through our simulations. Since 8 different MCS's defined for this standard, we got total of 32 different transmission parameters. Among these transmission parameters, we chose subset of 13 transmission schemes as they provide highest throughput under the certain BER threshold which we chose considering quality-of-service dependent applications. According to the simulation results, the use of dual-polarized antennas with the adaptive algorithm provide a double throughput and a significant coverage increase over conventional systems for 802.11n systems. One

can easily see the throughput and range improvement for other next-generation wireless networks via simulations.

APPENDIX A: DERIVATION OF EQUATIONS (4.23) AND (4.24)

In order to find ϕ_l, we first need to get the following equation.

$$\begin{aligned} E[z_l u_l^*] &= \mathrm{E}\Big[(\phi_l u_l + n_l)u_l^*\Big] \\ &= \phi_l \varepsilon_{av} \end{aligned} \tag{A.1}$$

$$\begin{aligned} \phi_l &= \frac{1}{\varepsilon_{av}}\mathrm{E}[\mathbf{w}_i^H \widetilde{\mathbf{r}} u_l^*] \\ &= \frac{1}{\varepsilon_{av}}\mathrm{E}\Big[\Big(\mathbf{w}_i^H \mathbf{H}(\mathbf{u} - \overline{\mathbf{u}}_i) + \mathbf{w}_i^H \mathbf{n}\Big)u_l^*\Big] \\ &= \frac{1}{\varepsilon_{av}}\mathrm{E}\Big[\mathbf{w}_i^H \mathbf{H}\mathbf{u} u_l^*\Big] \\ &= \frac{1}{\varepsilon_{av}}\mathbf{w}_i^H \mathbf{H}\mathbf{e}_i \end{aligned} \tag{A.2}$$

$$\begin{aligned} \sigma_k^2 &= \mathrm{E}\Big[(z_l - \phi_l u_l)(z_l - \phi_l u_l)^*\Big] \\ &= \mathrm{E}[z_l z_l^*] - \phi_l^2 \varepsilon_{av} \\ &= \mathrm{E}[\mathbf{w}_i^H \mathbf{r}\mathbf{r}^H \mathbf{w}_i] - \phi_l^2 \varepsilon_{av} \\ &= (\phi_l - \phi_l^2)\varepsilon_{av} \end{aligned} \tag{A.3}$$

REFERENCES

1. Alamouti S. M., "A simple transmitter diversity scheme for wireless communications," *IEEE Journal on Selected Areas in Communication*, vol. 16, pp. 1451-1458, Oct. 1998.

2. Tarokh V., H. Jafarkhani, and A. R. Calderbank, "Space-time block coding for wireless communications: Performance results," *IEEE Journal on Selected Areas in Communication*, vol. 17, no. 8, pp. 451-460, Mar. 1999.

3. Foschini G. J., "Layered space-time architecture for wireless communication in a fading environment when using multi-element antennas," *Bell Labs Technical Journal*, pp. 41-59, Autumn 1996.

4. Oestges C., B. Clerckx, M. Guilland, and M. Debbah, "Dual polarized wireless communications: From propagation models to system performance evaluation," *IEEE Transactions on Wireless Communication*, vol. 7, no. 10, pp. 4019-4031, May 2005.

5. Nabar R. U., H. Bölcskei, V. Erceg, D. Gesbert, and A. J. Paulraj, "Performance of multiantenna signaling techniques in the presence of polarization diversity," *IEEE Transactions on Signal Processing*, vol. 50, no. 10, pp. 2553-2562, Oct. 2002.

6. Wang X. and H.V. Poor,"Iterative (turbo) soft interference cancellation and decoding for coded CDMA,"*IEEE Transactions on Communication*, vol.47, pp. 1046-1061, July 1999.

7. Lu B. and X. Wang, "Iterative receivers for multiuser space-time coding systems," *IEEE Journals on Selected Areas in Communication*, vol. 18, no. 11, pp. 2322-2332, Nov. 2000.

8. Abe T. and T. Matsumoto, "Space-time turbo equalization in frequency-selective MIMO channels," *IEEE Transactions on Vehicular Technology*, vol. 52, no. 3, pp. 469-475, May 2003.

9. Tüchler M., R. Koetter and A. C. Singer, "Turbo equalization: Principles and new results," *IEEE Transactions on Communication*, vol. 50, no. 5, pp. 754-767, May 2002.

10. Tüchler M., A. C. Singer and R. Koetter, "Minimum mean squared error equalization using a priori information," *IEEE Transactions on Signal Proccesing.*, vol. 50, no. 3, pp. 673-683, March 2002.

11. Pancaldi F. and G. M. Vitetta, "Frequency domain equalization for space-time block-coded systems," *IEEE Transactions on Wireless Communication*, vol. 4, no. 6, pp. 2907-2916, Nov. 2005.

12. Tüchler M. and J. Hagenauer, "Linear time and frequency domain turbo equalization," in *Proceedings of IEEE Vehicular Technology Conference (VTC Spring 2001)*, pp. 1449-1453, May 2001.

13. Li B., D. Yang, X. Zhang and Y. Chang, "Turbo frequency domain equalization for single carrier space-time block coded transmissions," in *Proceedings of IEEE Global Communication Conference*, Dec 2008, pp. 1-5.

14. Al-Dhahir N., "Single-carrier frequency domain equalization for space-time block coded transmission over frequency selective fading channels," *IEEE Communication Letters*, vol. 5, pp. 304-306, July 2001.

15. Eşli C., M. Koca and H. Deliç, "Iterative joint tone-interference cancellation and decoding for MIMO-OFDM," *IEEE Transactions on Vehicular Technology*, vol. 57, pp. 2843-2855, Sept. 2008.

16. Zuyderhoff D., X. Wautelet, A. Dejonghe and L. Vandendorpe, "MMSE turbo

receiver for space-frequency bit-interleaved coded OFDM," in *Proceedings of IEEE Vehicular Technology Conference (VTC Fall 2003)*, pp. 567-571, Oct. 2003.

17. Forenza A., A. Pandharipande, H. Kim and R. W. Heath, "Adaptive MIMO transmission scheme: Exploiting the spatial selectivity of wireless channels," in *Proceedings of IEEE Vehicular Technology Conference (VTC Spring 2005)*, pp. 3188-3192, May-June 2005.

18. Tarokh V., N. Seshadri, and A. R. Calderbank, "Space-time codes for high data rate wireless communication: Performance criterion and code construction," *IEEE Transactions on Information Theory*, vol. 44, no. 2, pp. 744-765, Mar. 1998.

19. Oestges C. and B. Clerckx, *MIMO Wireless Communications From Real World Propagation To Space-Time Code Design*, Elsevier Ltd., Great Britian, 2007.

20. Kermoal J. P., L. Schumacher, K. I. Pedersen, P. E. Mogensen, and F. Frederiksen, "A stochastic MIMO radio channel model with experimental validation," *IEEE Journals on Selected Areas in Communication*, vol. 20, no. 6, pp. 1211-1226, Aug. 2002.

21. Vucetic B. and J. Yuan, *Space-Time Coding*, John Wiley and Sons Ltd., 2003.

22. Biglieri E., R. Calderbank, A. Constantinides, A. Goldsmith, A. Paulraj and H. V. Poor, *MIMO Wireless Communications*, Cambridge University Press, United Kingdom, 2007.

23. Lee W. C. Y. and Y. S. Yeh, "A polarization diversity system for mobile radio," *IEEE Transactions on Communications*, vol. Com-20, no. 5, pp. 912-923, Oct. 1972.

24. Larsson E. G. and P. Stoica, *Space-Time Block Coding for Wireless Communications*, Cambridge University Press, 2003.

25. Lindskog E. and A. Paulraj, "A transmit diversity scheme for channels with inter-

symbol interference," in *Proceedings of IEEE International Conference on Communications*, vol. 1, New Orleans, June 2000, pp. 307-311.

26. Tarokh V., H. Jafarkhani and A. R. Calderbank "Space-time-block codes from orthogonal designs," *IEEE Transactions on Information Theory*, vol. 45,no. 5, pp. 1456-1467, July 1999.

27. Nee R. V. and R. Prasad, *OFDM For Wireless Multimedia Communications*, Artech House , USA, 2000.

28. Clerckx B., L. Vandendorpe, D. Vanhoenacker-Janvier, and A. J. Paulraj, "Robust space-time codes for spatially correlated MIMO channels," *IEEE International Conference on Communications*, vol. 1, pp. 453-457, 20-24 June 2004

29. Weichselberger W., M. Herdin, H. Özçelik and E. Bonek, "A stochastic MIMO channel model with joint correlation of both link ends," *IEEE Transactions on Wireless Communication*, vol. 5,no. 1, pp. 90-100, Jan. 2006.

30. Deng Y., A. Burr, and G. White, "Performance of MIMO systems with combined polarization multiplexing and transmit diversity," In *Proceedings of IEEE Vehicular Technology Conference (VTC Spring 2005)*, pp. 869-873, May 2005.

31. Naguib A., N. Seshadri and A. R. Calderbank, "Increasing data rate over wireless channels," *IEEE Signal Processing Magazine*, pp. 76-92, May 2000.

32. Berrou C., A. Glavieux and P. Thitimajshima, "Near shannon limit error-correction coding and decoding: Turbo codes," in *Proceedings of International Conference on Communications*, pp. 1064-1070, 1993.

33. Douillard C., M. Jezequel, C. Berrou, A. Picart, P. Didier and A. Glavieux, "Iterative correction of intersymbol interference: Turbo equalization," *European Transactions on Telecommunications*, vol. 6, no. 5, pp. 507-511, Sept. - Oct. 1995.

34. Reynolds D., X. Wang, "Low complexity turbo-equalization for diversity chan-

nels,"*Signal Processing*, vol. 81, no. 5, pp.989-995, 2001.

35. Laot C., R. L. Bidan and D. Leroux, "Low complexity MMSE turbo equalization: A possible solution for EDGE," *IEEE Transactions on Wireless Communications*, vol. 4, no. 3, pp. 965-974, May. 2005.

36. Viterbi A. J., "An intuitive justification and a simplified implementation of the MAP decoder for convolutional codes," *IEEE Journals on Selected Areas in Communication*, vol. 16, no. 2, pp. 260-264, Feb. 1998.

37. Robertson P., E. Villebrun and P. Höher, "A comparison of optimal and sub-optimal MAP decoding algorithms operating in the log domain," in *Proceeding of IEEE International Conference on Communications*, pp. 1009-1013, June 1995.

38. Bahl L. R., J. Cocke, F. Jelinek, and J. Raviv, "Optimal decoding of linear codes for minimizing symbol error rate," *IEEE Transactions on Information Theory*, vol. IT-20, no. 2, pp. 284-287, March 1974.

39. Catreux S., V. Erceg, D. Gesbert and R. W. Heath,"Adaptive modulation and MIMO coding for broadband wireless data networks," *IEEE Communications Magazine*, vol. 40, no. 6, pp. 108-115, June 2002.

40. Kamerman A. and L. Monteban, "WaveLAN-II: A High-performance wireless LAN for the unlicensed band", *Bell Labs Technical Journal*, pp. 134-140, Summer 1997.

41. Lacage M., M. H. Manshaei and T. Turletti, "IEEE 802.11 rate adaptation: A practical approach," in *Proceedings of 7th ACM International Symposium on Modeling, Analysis and Simulation of Wireless and Mobile Systems*" Venezia, pp. 126-134, 2004.

42. Kim J., S. Kim, S. Choi and D. Qiao, "CARA: Collision-aware rate adaptation for IEEE 802.11 WLANs," in *Proceedings of IEEE International Conference on Computer Communications*, pp. 1-11, April 2006.

43. IEEE P802.11n/D4.00, "Wireless LAN medium access control (MAC) and physical layer (PHY) specifications: Amendment 4: Enhancements for higher throughput," March 2008.